Master of Science
Thesis
VT2023

Uncertainties in the use of synthetic CT (sCT) for daily online adaptive radiotherapy for lung cancer

Vivika Johansson

Supervisors

Wiviann Ottosson and Patrik Sibolt

Medical Radiation Physics, Lund
Faculty of Science
Lund University
www.msf.lu.se

Popular scientific summary in Swedish

Lungcancer har den högsta dödligheten för cancerrelaterade sjukdomar och är vanligare hos kvinnor än hos män. Under 2021 rapporterade cancerfonden att 4264 personer i Sverige hade insjuknat i lungcancer varav 2352 var kvinnor och 1912 var män. De senaste åren har prognosen för lungcancer förbättrats markant, där fler och fler blir långtidsöverlevare. Prognosen har framför allt förbättrats på grund tidig detektion och förbättrade behandlingstekniker. Den främsta orsaken till lungcancer är rökning på grund av cancerframkallande föreningar som finns i tobak.

Tillgängliga behandlingsmetoder är operation, strålbehandling och läkemedel. Strålbehandling är en av de vanligaste behandlingsmetoderna mot cancer, det innebär att en liten mängd stråldos levereras till tumören för att döda cancerceller över en period. Normalt har lungcancerpatienter 30 till 33 fraktioner. Inför strålbehandling ska en del förberedelse göras, det innebär att patient ska genomgå datatomografi även kallad för CT. Datatomografi ger en tredimensionell bild över behandlingsområdet och information hur röntgenstrålning dämpas i kroppen. I sin tur används CT-bilden för att skapa en behandlingsplan och beräkna stråldos till tumör och friska organ. Varje patient får en behandlingsplan skräddarsydd för dem, för att ge den mest optimala behandlingen. Inför varje behandling tas en tvådimensionell röntgenbild som kallas för Cone beam computer tomography (CBCT). CBCT-bilden används för att kunna positionera patienten rätt, med andra ord säkerställs det att tumören träffas av strålningen. Anatomiska förändringar kan detekteras på CBCT-bild och om de har förändrats drastiskt behöver patienten genomgå ett ytterligare CT-undersökning för att skapa en ny behandlingsplan, kallad för re-planning plan. De anatomiska förändringarna förekommer hos lungcancerpatienter och det som kan inträffa är atelektas, pleuravätska, lunginflammation, tumörminskning eller att tumörens position ändras. Beroende på hur patienten och anatomiska förändringar ser ut kan den planerade behandlingsplanen vara bättre eller sämre anpassad till patienten, detta problem kan undvikas med adaptiv strålbehandling.

Adaptiv strålbehandling är en alternativ behandlingsmetod som tar hänsyn till den dagliga anatomin och anpassar dosplanen enligt patients anatomiska utseende. För att kunna utgöra en dosberäkning i den adaptiva strålbehandlingen används syntetisk CT kallad för sCT. sCT skapas från den dagliga CBCT-bild med beräkningsinformation, så kallad Hounsfield Unit (HU) från planering CT. HU ger information hur strålningen dämpas i kroppen. Det finns en oro över hur dessa sCT hanterar stora anatomiska förändringar i adaptiv strålbehandling och hur stor den dosimetriska osäkerheten kan bli. Vid tillfällen där det finns stora anatomiska förändringar hos lungcancerpatienten kan överföring av HU från planering CT till den dagliga CBCT-bild skapa en stor osäkerhet för densitetsmappning på den sCT bild, och det kan leda till avvikande dosberäkning.

Det andra möjliga alternativ för att göra en dosberäkning i en adaptiv plan, är att dosberäkna på CBCT-bild som tas inför varje behandlingstillfälle. Syftet med detta projekt undersöker om dosberäkning på CBCT-bild minskar det dosimetriska osäkerheter i jämförelse med dosberäkning av sCT vid stora anatomiska förändringar för lungcancerpatienter. De sCT bilder ska utvärderas om det erinra med re-planning CT i hänsyn med de stora anatomiska förändringarna.

Abstract

Background and purpose: Cone Beam Computed Tomography (CBCT) based online adaptive radiotherapy (oART) has been clinically implemented for several anatomical sites worldwide. However, random and abrupt anatomical changes with large density alterations can occur in lung patients, leading to uncertainties with synthetic computed tomography (sCT) and dose calculation. The anatomical changes could be the resolution/appearance of atelectasis, tumor shrinkage, tumor positional deviation, pleural effusion, pneumonitis, etc. This study aimed to quantitatively investigate the uncertainty of dose calculation on sCT in the Ethos (Varian Medical Systems, Palo Alto, CA) oART-workflow and the possibility of using direct dose calculation on CBCT to minimize the dosimetric uncertainties for lung cancer patients with a broad range of anatomical changes. As well as qualitatively observe the generated sCT images.

Methods: Twenty lung cancer patients with different anatomical changes, resulting in re-planning during their courses of treatment, were included (treated between 15 January 2018 and 15 December 2022). An oART workflow was simulated for each patient in an Ethos emulator running in batch mode (Varian Medical Systems). During the simulated oART sessions, the original planning CT (pCT) was deformed to the re-planning CT (rCT), and also deformed to the first CBCT post-re-planning, used as input for the anatomy-of-the-day, generating the $sCT_{\mathbf{rCT}}$ and sCT_{CBCT}, respectively. The rCT treatment plan was re-calculated on the generated sCT_{rCT}, sCT_{CBCT}, and directly on each patient's CBCT (dCBCT). Resulting dose distributions were compared with the rCT using relevant dose volume histogram (DVH) parameters, where the dosimetric agreement was evaluated using Wilcoxon signed rank testing.

Results: 12 out of 20 generated sCT_{rCT} and 14 out of 20 sCT_{CBCT} images were assessed to have an anatomical disagreement with rCT due to anatomical changes that could not be corrected for by deformation in the Ethos oART workflow. The DVH differences between rCT-sCT_{rCT} (in 13 out of 20 patients) and rCT-sCT_{CBCT} (in 11 out of 16 patients, four patients were excluded due to large anatomical disagreement between CBCT and rCT) were acceptable (within 2.0%). The rest of the patients resulted in higher (over 2.0%) dose differences for any dosimetry metric investigated due to incorrect image deformations and erroneously generated sCTs because of anatomical changes.
The DVH dosimetry metric differences in rCT-sCT_{rCT} (median, [min; max]) for the target structures were 0.3 [-2.0; 4.0]%, 0.3 [-0.2; 3.4]%, and -0.4 [-7.8; 0.9]% for GTV $D_{99\%}$, PTV $D_{98\%}$ and PTV D_{max}, respectively. In contrast, the corresponding differences for organs at risk (OAR) were 0.0 [-0.2; 0.1]%, 0.0 [-0.3; 0.2]%, 0.0 [-0.7; 1.0]%, 0.0 [-1.1; 0.5]% and -0.4 [-7.2; 2.0]% for mean lung dose (MLD), esophagus mean dose (D_{mean}), heart V_{25Gy}, spinal cord maximum dose (D_{max}) and body D_{max}, respectively. The Wilcoxon signed rank presented statistically significant differences between rCT-sCT_{CBCT} and rCT-sCT_{rCT}, where DVH differences for rCT-sCT_{CBCT} were -1.3 [-9.0; 1.4]% and -1.0 [-8.1; 1.4]% in comparison to rCT-sCT_{rCT} with -0.4 [-7.8; 0.9]% and -0.4 [-7.2; 2.0]% for PTV D_{max} and body D_{max}, respectively.
The corresponding DVH differences between dCBCT and rCT were 1.1 [-1.3; 5.1]% for PTV $D_{98\%}$, and OAR, the differences were -1.9 [-6.8; -0.1]%, -7.2 [-15.2; 1.6]%, -1.7 [-27.1; 7.6]%, -0.7 [-7.4; 4.7]%, and -2.2 [-5.7; 4.3]% for MLD, esophagus D_{mean}, heart V_{25Gy}, spinal cord D_{max} and body D_{max}, respectively.

Conclusions: Anatomical disagreement between sCTs and rCT images for lung cancer patients with anatomical changes could cause dose differences of over 2.0%. However, this is not always the case, and therefore this type of patient cohort with anatomical changes undergoing oART must be carefully evaluated on a patient individual level. This finding demonstrates the need for patient and fraction-specific quality assessment, which is unavailable in the current version of Ethos treatment system.
The future solution could potentially be direct dose calculation on CBCT. However, this requires further investigation since no conclusion can be drawn from this study due to rCT and CBCT geometrical differences. The findings in this study suggest that using the oART workflow with the Ethos treatment system for lung cancer patients with anatomical changes is currently not clinically appropriate due to the uncertainties with the resulting sCT used for the oART workflow.

Acknowledgments

Firstly, I would like to express my gratitude and appreciation to my supervisors:

Wiviann Ottosson, thank you for your guidance and wise suggestions for this project. You have been an incredible help and a great motivation at every step of this project.

Patrik Sibolt, thank you for your support and guidance. Your wise suggestions and directions are invaluable and helped me on the right track when feeling lost.

A special thank you to the Varian team, who helped generate sCTs and gave valuable input to this study.

Lastly, I would like to thank my friends, classmates and family for motivating me and giving endless support during this project.

List of abbreviations (Alphabetical order)

ART	Adaptive radiotherapy
Ate	Atelectasis
CBCT	Cone beam computed tomography
CTV	Clinical target volume
dCBCT	direct dose calculation on CBCT
DIBH	Deep-inspiration, breath-hold
DIR	Deformable image registration
DOF	Degree of freedom
DVH	Dose Volume Histogram
FB	Free breathing
FOV	Field of view
GTV	Gross tumor volume
HU	Hounsfield Units
IMRT	Intensity-modulated radiation therapy
NSCLC	Non-small cell lung cancer
oART	Online Adaptive radiotherapy
paCBCT	pre-adaption CBCT
PL	Pleural effusion
Pne	Pneumonitis
ptCBCT	pre-treatment CBCT
PTV	Planning target volume
RIR	Rigid image registration
RT	Radiotherapy
SBRT	stereotactic body radiation therapy
SCLC	Small cell lung cancer
sCT	Synthetic computer tomography
sCT_{CBCT}	sCT generated from deforming pCT to CBCT
sCT_{rCT}	sCT generated from deforming pCT to rCT
TPD	Tumor positional deviation
TPS	Treatment planning system
TS	Tumor shrinkage
QA	Quality Assurance

Table of content

1. Introductions

Lung cancer is one of the most common types of cancer and has a high mortality rate. For the past several years, lung cancer's survival rate has increased, mainly due to advancements in treatment, availability of screening, and early detection. [1] Smoking is the primary risk factor for lung cancer; other factors such as age, radon exposure, gender, race, pre-existing lung diseases, and environmental pollution are also important. [2]

Lung cancer tumors are categorized into two broad histologic classes **Non-Small Cell Lung cancer (NSCLC)** and **Small Cell Lung cancer (SCLC)**. NSCLC is the most common type of lung cancer. Approximately 80 - 85% of lung cancer tumors are NSCLC, and 15-20% are SCLC. [1]

Types of treatment for lung cancer include external beam radiotherapy (RT), surgery, targeted therapy, chemotherapy, or palliative care. The direction of treatment is mainly dependent on the stage of cancer. RT is one of the treatment modalities used independent of the tumor stage, and around 77% of all lung cancer patients have indications of needing RT at some point in their treatment. [3, 4]
Thoracic RT can last between 5-6 weeks, where the patient's treatment plan is based on a Computer Tomography (CT) scan of the patient's anatomy at the beginning of RT. However, weight loss, tumor response, and anatomical changes are expected during the treatment course. The anatomical changes include tumor shrinkage (TS), tumor positional deviation (TPD), resolution or appearance of atelectasis (Ate), pleural effusion (PE), and pneumonitis (Pne), which can occur abruptly during the treatment course. Sometimes the anatomical change is severe and requires a re-planning scan and new treatment plan, which can be time-consuming for both the clinic and the patients. [5]
Clinical evidence suggests thoracic RT-induced heart disease causes risk for pneumonitis and other cardiac and pulmonary radio-induced side effects. [6, 7]

The improvement of lung cancer treatment has grown notably. Better utilization of radiation planning and delivery systems has made it possible for a conformal delivery of radiation, such as intensity-modulated radiation therapy (IMRT), stereotactic body radiation therapy (SBRT), and proton therapy. In addition, the advancement in technology with image modality availability during planning and treatment has made it possible to adapt tumor volume (target volume) within the session and between fractions, and this is called adaptive radiotherapy (ART).[8] The treatment method has developed into adapting every fraction during treatment, called online adaptive radiotherapy (oART).
Many clinics worldwide have clinically implemented cone beam computed tomography (CBCT)-guided oART. CBCT-guided oART is feasible for treatment in pelvic regions such as prostate, anal, bladder, and cervical cancer. [9–13] The interest in expanding the treatment sites for oART for targets above the diaphragm, such as head and neck, and lung sites has increased when clinical experience with oART has gained. A study from Hoegen et al. [14] and Dial et al. [15] states that ART for lung cancer patients decreases the dose to the lung, heart, and esophagus but not significantly. The importance of a daily CBCT image acquisition was highlighted by Møller et al. [16] to identify the different anatomical changes in lung cancer patients. These changes can occur abruptly and randomly during the treatment course, and according to Møller et al., half of the patients with an anatomical change could benefit from ART.
Ethos therapy is a Varian Adaptive Intelligence ((Varian Medical Systems) solution that allows for oART using artificial intelligence (AI) and machine learning for contour and adapted plan generation while the patient is on the treatment couch. [17]
Due to the limited image quality of the current version of CBCT images on Ethos machines, it is not possible to calculate the absorbed dose correctly on the CBCT image. Therefore, for the oART workflow, the Ethos therapy system uses AI and deformable image registration (DIR) to generate synthetic Computed Tomography (sCT) images used for absorbed dose calculation. There are uncertainties with DIR; the sCTs inherently contain uncertainties when mapping Housfield units (HUs) during the sCT generation. These uncertainties are most profound for large density alteration cases, such as lung cancer patients with large anatomical changes.

1.1 Project aim

For lung cancer patients with large anatomical changes, this project aimed to investigate the uncertainties related to the use of daily CBCT-guided AI-driven oART. This study hypothesized that the use of direct dose calculation on CBCT would reduce uncertainties compared to the use of sCT for absorbed dose calculation in the presence of large density alterations caused by anatomical changes. This was investigated by using the Ethos therapy system:

- Evaluating the reliability of using sCT images for patients with large anatomical changes for absorbed dose calculation in an oART setting; by observation of the geometrical information and anatomical agreement between the re-planning CT (rCT) and the sCTs, which were generated from deforming planning CT (pCT) to rCT and to the first CBCT post-re-planning acquired the fraction after the rCT.

- Quantitative dose comparison between the rCT treatment plan and the re-calculated rCT treatment plan on CBCT (dCBCT), $sCT_{rCT,}$ and sCT_{CBCT}.

2. Theory

2.1 Conventional and online ART Delivery Workflow

Radiation treatment can be delivered in the conventional ART or oART workflow. Currently, conventional ART is implemented for lung cancer patients, and there is no clinical oART protocol for lung cancer patients treated at Ethos linac at Herlev Hospital. However, real-time tracking and oART are offered on the MR linac, where the beam is triggered by the position of the tumor for very centrally positioned lung SBRT targets, included in the STAR protocol. [18]

2.1.1 Conventional Workflow

In general, conventional RT treatment consists of treatment planning with a planning image of the disease site, and depending on tumor location, different image modality is utilized (MRI, CT, or PET/CT). Firstly, for lung cancer patients, treatment planning is based on a CT image called planning CT (pCT). Depending on the tumor movement measured in a respiratory correlated CT scan (4DCT) during simulation, the patient receives a free-breathing (FB) or deep-inspiration breath-hold technique (DIBH).

Secondly, physicians delineated targets such as gross tumor volume (GTV), clinical tumor volume (CTV), planning target volume (PTV), and OAR in a treatment planning system (TPS). Thirdly, dose calculation is applied to deliver the prescribed dose to the target and spare normal tissue. Lastly, patient-specific QA is conducted before the patient begins treatment. Figure 1 summarizes the conventional RT workflow. Inside the treatment room, the patient lies on the couch and is correctly positioned before treatment with a daily CBCT acquired for online soft tissue tumor matches with pCT using RIR.

An anatomical change is detected during the daily CBCT image acquisition procedure for some patients, affecting their treatment and radiation delivery since their current treatment plan is insufficient and requires a re-scanning CT (rCT) and a new dose calculation.

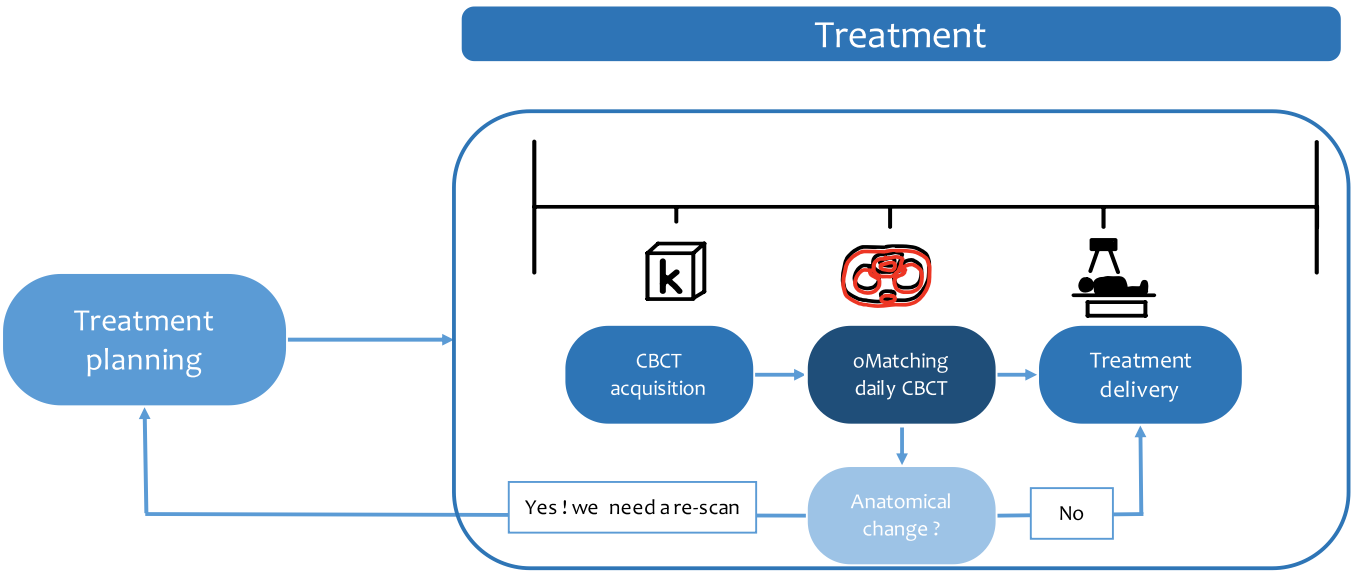

Figure 1: Conventional workflow consists of initial treatment planning, pre-treatment, and, during treatment, a CBCT acquisition with online matching for setup and evaluation of anatomical changes. If systematic anatomical changes occur during treatment, a re-scan and re-planning process is initiated.

2.1.2 Dose calculation on Synthetic Computed Tomography (sCT)

Synthetic Computed Tomography (sCT) or pseudo-CT for dose calculation has quickly become vital to RT. [19] One way to utilize the sCT is in the MRI-only RT workflow, where promising results are presented for accurately calculating the absorbed dose in the prostate, brain, thorax, and head and neck treatment sites in an MRI-only RT workflow. [19–21] sCT in the MRI-only workflow is preferred over conventional CT in delineating target and OAR due to superior image quality in soft tissue contrast. Usually, in a conventional RT, the absorbed dose calculation is based on CT, which converts HU to relative electron density in the TPS. In an MRI-only RT workflow, where no CT image is acquired, it is difficult to perform a dose calculation on the absorbed dose since MRI has no physical quantity, and as a result, a sCT is necessary.[19]

Another way to utilize the sCT is in the ART workflow. The same idea applies to the dose calculation on the sCT generated in the oART workflow, where the original pCT deformed to fit the daily acquired CBCT as the input of the daily anatomy, creating a greyscale volume called density map or sCT. The density map is essential for both MR-guided and CBCT-guided oART.
The oART clinical experience with Ethos therapy for anal and bladder cancer, described by Åström et al.[12, 22] and Sibolt et al.[11] demonstrate the possibility of reducing the target margin and potentially reducing toxicity for anal and bladder cancer, respectively.

2.1.3 oART workflow in Ethos

The procedure in a daily CBCT-guided oART with AI-driven adaptive treatment workflow using Ethos requires minimal manual input from the user and is automated for the most part. The workflow is divided into three procedures:

- initial planning (treatment planning)
- on-couch adaption
- treatment monitoring

Firstly, in the initial planning step, a plan template is chosen for the anatomical site with the physician's intent describing the prescribed dose to target and OAR constraints. The constraints are priority-based, where the most critical constraints are set with the highest priority, and these constraints are referred to

as planning directives. The planning directives automatically generate a plan for online and offline ART with help from the Intelligent Optimization Engine (IOE). The engine is an algorithm managing plan optimization and generates several IMRT and Volumetric Modulated Arc Therapy (VMAT) with different options for beam geometries. Plan comparison is made in the Ethos treatment planning system (TPS), where the user selects the reference plan.

The second step is the on-couch adaptation (Figure 2).

1. Image acquisition of a pre-adaptation CBCT (paCBCT) is used for treatment setup and image quality evaluation, and depending on the anatomical site, different *influencers* are activated. Influencers are structures generated close to the target; in some cases, influencers are the target. They are used to create a structure-guided deformable image registration between the pCT and acquired CBCT scans. Depending on the anatomical site, the influencers can be AI-segmented or elastically propagated by DIR (if located over the diaphragm) from the pCT onto the sCT, generated from the daily CBCT as an anatomy-of-the-day input. The influencers are evaluated and manually edited if necessary.
2. Contour evaluation of the target propagation is based on the influencer segmentation (since the DVF is based on the segmentation of influencers, it will affect the target propagation). In the case of a lung cancer patient with a tumor in the lung lobe, the influencer segmentation with the target will heavily affect the target propagation due to overlap. If there is more than 50% overlap between the influencer and target, the target propagation is done by structure-guided DIR. Otherwise, a B-spline model is optimized for target propagation by so-called elastic DIR. The algorithm propagates the CTV from the pCT to the generated sCT based on the daily acquired CBCT, and the PTV is derived from CTV by expanding the margin. The target contour is evaluated and accepted before the next step.
3. In the third step, based on the daily anatomy and target propagation, Ethos TPS generates two plans. One is the *scheduled plan*, where the original treatment plan is re-calculated based on the anatomy of the day. For the *adapted plan*, the reference plan is re-optimized by the IOE, also based on the anatomy of the day. In the background, a sCT or a so-called "density map" is generated by deforming the pCT to the daily CBCT used for the dose calculations.
4. At the plan report, the user receives an overview of monitor units (MU) and the quality of the sCT. Before the treatment is initiated, patient-specific QA is performed where the plan, image, and contours are sent to Mobius 3D, an independent dose verification software, to compare clinical goal metrics, dose distribution, 3D gamma analysis, and Dose-Volume Histogram (DVH). DVH relates radiation dose to a volume set in the radiation therapy planning.
5. Before the treatment is delivered, another optional CBCT is acquired, denoted pre-treatment CBCT (ptCBCT), used to evaluate possible anatomical changes happening between pre-adaptation until just prior to treatment, including intra-fractional uncertainties. Intra-fractional uncertainty is the motion of anatomy during the treatment session.
6. Lastly, the treatment is delivered.

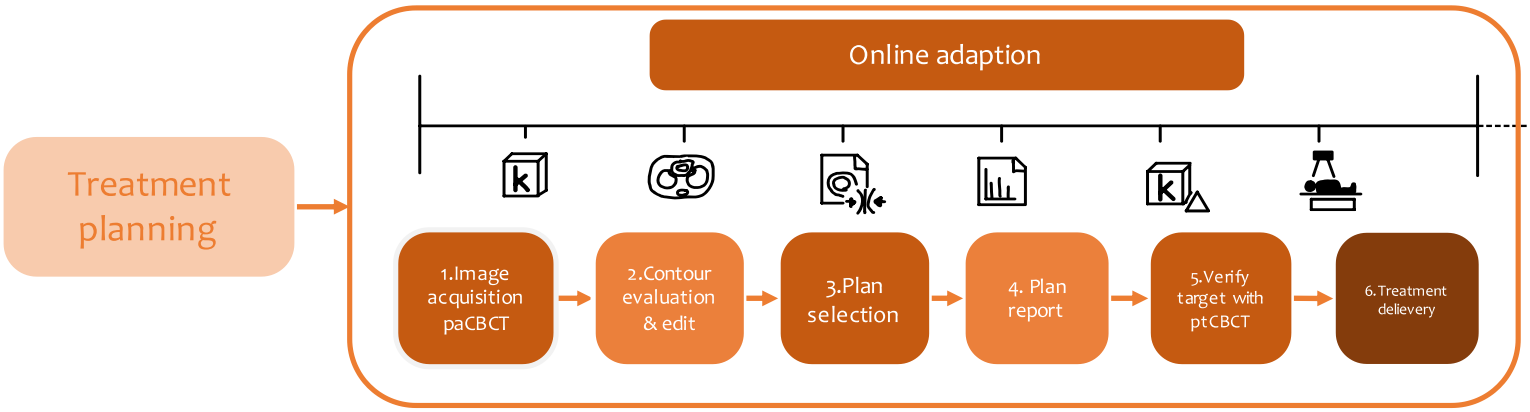

Figure 2: oART workflow steps for treatment planning. (1) CBCT acquisition, (2) contour evaluation, (3) plan selection, (4) plan report, (5) verification target with CBCT, (6) and treatment delivery.

2.1.4 sCT generation in Ethos

Varian refers to sCT as a density map; however, for the project's simplicity, it will be referred to as sCT. sCT generates from deforming the pCT to the daily CBCT with DIR. As a result, in the areas where pCT and CBCT overlap, the HU value from pCT is deformed to CBCT anatomy and generates a new greyscale volume for dose calculation. The HU values are based on the daily anatomy of the CBCT. Image registration and DVF are fundamental processes in density mapping. Any error in image registration and image quality can affect density mapping and, therefore, dose calculation. Stitching artefacts are prevalent for sCT from deforming planning CT to CBCT since CBCT field of view (FOV) is smaller than pCT, or the patient body contour has changed during the treatment period (Figure 3) .

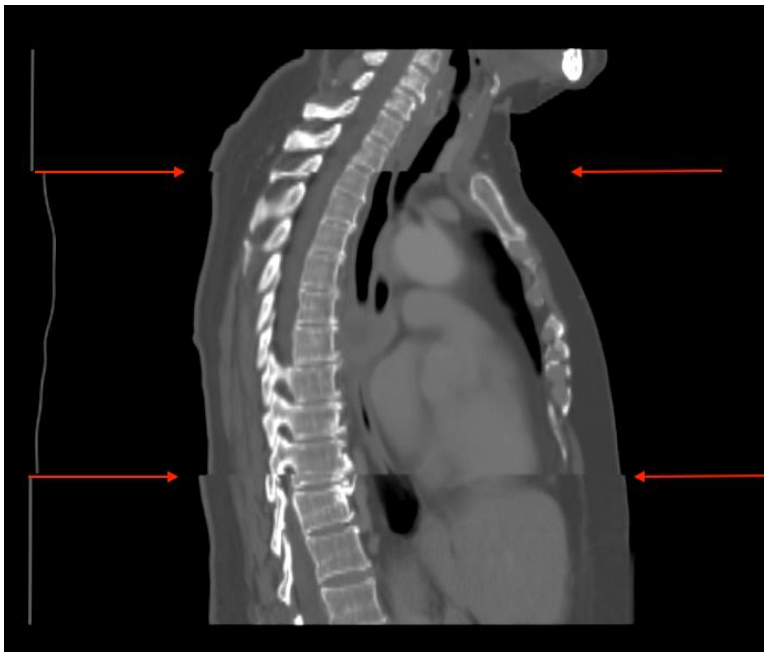

Figure 3: sCT with stitching artefacts illustrated with red arrows.

2.2 Image registration: B-spline and elastic image registration

The influencer structure and target propagation in Ethos workflow (Figure 2) utilized different image registration methods depending on whether the influencer structure is an AI segment and if the target is inside the CBCT FOV, etc. The important image registration method in this project is B-spline and elastic deformable image registration.

Image registration is a process that finds the spatial correspondence between two image sets, one is called a reference image (fixed), and the other image set is a template image that you want to transform so it becomes similar to the reference image geometrically. In conventional RT, the treatment image (CT or MRI) is considered a reference image, while the template image is a CBCT of the daily anatomy acquired before treatment. [23]

Image registration can either be rigid or non-rigid. In a rigid image registration (RIR), all pixels can be translated or rotated in six degrees of freedom (6DOF). In conventional RT, RIR works well for non-anatomical changes, such as bony matches used for patient setup. The non-rigid or deformable image registration (DIR) has more DOF and is a better method to handle anatomical changes such as shifting, skewing, and non-linear shrinking or expansion because DIR can handle local distortion. DIR algorithms

include an objective function with some similarity metric, an optimization method that controls the transformation to maximize the similarity metric, and a deformation model with some regularization so only smooth and realistic deformations are accepted. The DIR results in a deformable vector field (DVF) that describes the spatial relation for each voxel between the template and reference image.

There are different methods of DIR, and the most relevant for this project is the B-spline registration. DIR uses the B-spline (bell function) to define the continuous deformation field by mapping every voxel in the template image and the correspondence in the reference image. [24]
The definition of the B-spline curve (eq. 1) is described by the linear combination of control points, p_i , and the basis B-spline function, $\mathrm{N_{i,k}(t)}$. [25] The B-spline defines a flexible grid over the image where the grid nodes are called control points, p_i . The basis function is characterized by a knot vector *t* and is described in the equation (eq.1). The pro of utilizing the B-spline DIR is the computational efficiency when using a large number of control points. The mathematical property of the B-spline function becomes very useful by changing the control points, which results in local changes in the region (without affecting the global deformation). The spacing of control points can also be used to handle global rigid deformation by having a relatively large spacing of control points in contrast to local non rigid deformities, where a small spacing of control points is preferred. It is generally applicable for different purposes and computationally efficient. [26]

$$r(t) = \sum_{i=0}^{n} p_i N_{i,k}(t), \quad n \geq k-1, \qquad t \in [t_{k-1}, t_{n+1}] \qquad (\text{eq. } 1)$$

Another useful DIR in medical image analysis is elastic transformation, which is based on the model of elastic theory.[27] The model was originated by Broit [28]; the central idea was to match the objects with elastic transformation formulated as a minimization problem of the cost function. The cost function is way to measure the "goodness" of alignment. [29] There are various transformation approaches; one is based on landmarks such as points, curves, and surfaces, and the other is based on intensity. As a result, depending on the chosen strategy, elastic transformation extracts either a landmark or directly exploits intensity and computes a transformation based on the selected method. The idea of elastic transformation considers the images as continuous bodies to model the geometric differences between images and computes the local deformation quite well. [27] In other words, the elastic transformation can handle small and local shape changes; however, it fails if the global misalignment is enormous. [30] The computational aspect of elastic transformation is solved by the partial differential equation; once a global misalignment is introduced, it is difficult, computationally complex, and expensive to apply the flexible transformation for larger deformities. [30] The main difference between the B-spline and elastic deformation is the computational complexity, where the B-spline is less computationally demanding and offers a good local control of the deformities. On the other hand, elastic deformation is more computationally demanding and handles complex and continuous deformities. [26, 30]

2.3 Dose calculation on CBCT

The beam shape of the CBCT is shaped as a cone, and with a flat panel detector, an image of the treatment area can be obtained during the treatment session. In contrast, a spiral CT has a narrowly collimated fan-shaped X-ray beam and a linear collection of detectors where a 3D image can be obtained by moving the patient in a spiral direction (Figure 4). [31]

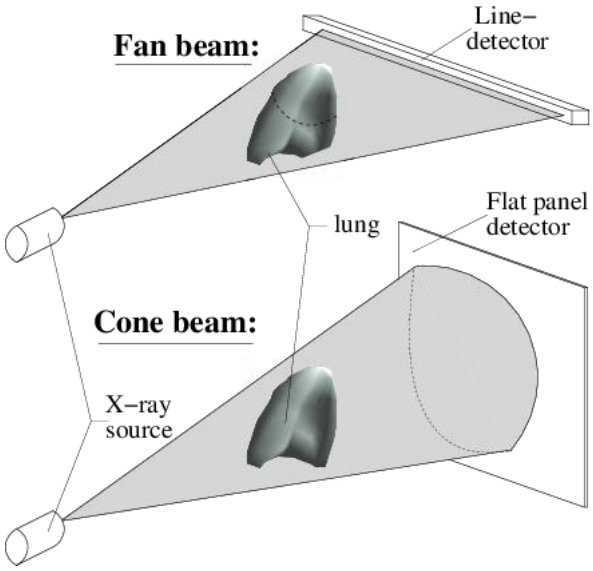

Figure 4: Illustration of fan beam from a CT with line detector (upper image) and cone beam for CBCT (lower image) with a flat panel detector along with X-ray source for different methods of image acquisition, Villard et.al. [32]

CBCT-based dose calculation is another approach to oART, applying a direct dose calculation on the CBCT image. The CBCT images are acquired pre-treatment for patient position verification, target, and OAR localization. Daily CBCT images are implemented for many institutions and are essential for treatment setup and detecting anatomical change. [33] The feasibility of CBCT-based dose calculation is a popular concept that would facilitate the oART-workflow.[34] It would eliminate an additional need for re-scanning CT and avoid uncertainties with sCT.
There are, however, a few concerns with using CBCT for dose calculation since CT and CBCT are two very different modalities. The difference between CBCT and CT includes the image acquisition parameters and image reconstruction techniques and, as a result, a discrepancy in image quality and HU.[34] CBCT has a poor image quality and inaccurate HU, where many studies have exhibited the need for HU correction to achieve a tolerable dosimetric evaluation between CT and CBCT plans. [35–37]
The study by De Smet et al. [35] included six lung cancer patients with doses calculated on CBCT where Hounsfield units-to-mass density correction tables were utilized. They demonstrated that the average differences were 2-3% for most dosimetry metrics using the standard HU-table and 1-2% dose differences using the HU-table specific for thorax CBCT. The other study by Kaplan et al. [36] used stoichiometric calibration to improve the accuracy of CBCT calculation for lung cancer patients. Kaplan et al. concluded that the dose calculation on CBCT of lung cancer patients was feasible within 4%. These two studies used different methods to improve the HU inhomogeneity and demonstrate a possible approach to dose calculation on CBCT in ART.

Another approach is mapping image densities from a CT to a CBCT by deformed image registration (DIR) to do dose calculations on an image set with correct relative electron density representation instead of a representation of HUs. This is the approach Ethos is utilizing in the oART workflow.
Cole et al. [38] conducted a retrospective study of seven lung cancer patients to propose using DIR to map the pCT to the daily CBCT image to investigate if a re-plan is necessary. Cole et al. used a simulated CBCT to minimize the anatomical differences due to rCT and CBCT acquisition from different image modalities and at different times. Later, the pCT was deformed to simulated CBCT to generate a deformed CT (dCT) to assess dose calculation. Cole et al. stated that the dCT dose assessment was similar to the gold standard of rCT. The max deviation for absolute dose difference for treated volume was less than 2.0% dose differences and less than 1.0% for organs at risk. The largest absolute dose deviation with re-calculation of rCT structure was at 2.0% for CTV+ 1cm $V_{95\%}$ (percentage of CTV +1 cm volume to receive 95% of the prescribed dose).

2.4 Types of Anatomical Changes in Lung Cancer Patients

Large anatomical changes can occur at any time for lung cancer patients during their treatment and result in a re-scan. The anatomical changes in this study include atelectasis, pneumonitis, and pleural effusion.

2.4.1 Atelectasis

Atelectasis occurs when there is a partial or complete collapse of the lung or lung lobe and when alveoli (lung sacs) are not inflating properly (collapse alveoli). In other words, oxygen may not reach blood cells, tissues, and organs. Atelectasis is often caused by pressure outside the lung, lack of airflow, scarring, or blockage and resolves when the underlying cause is treated. [39] Atelectasis can resolve on its own or shrink in size anytime during the radiation treatment, which causes the internal anatomy to alter (affecting both targets and organs at risk (OAR)). On a CT or CBCT, this typically looks like an increased density in the lung lobe, decreasing the lung lobe volume (Figure 5, a). This phenomenon can randomly appear and disappear during the course of treatment.[16]

2.4.2 Pneumonitis

Pneumonitis is an inflammation in air sacs in either one or both lungs caused by inflammation. Air sacs can be filled with fluid or purulent material, which causes fever, difficulty breathing, and cough with phlegm. [40] On a CT or CBCT, the affected area is denser and patchy (Figure 5, b).

2.4.3 Pleural effusion

The fluid accumulating in the pleural cavity between the parietal and visceral pleura is called pleural effusion. The cause arises from infection and malignancy of an inflammatory condition.[41]
On a CBCT or CT scan, this typically looks like the fluid is in the back of the patient when the patient lies down on the treatment couch (Figure 3, c).

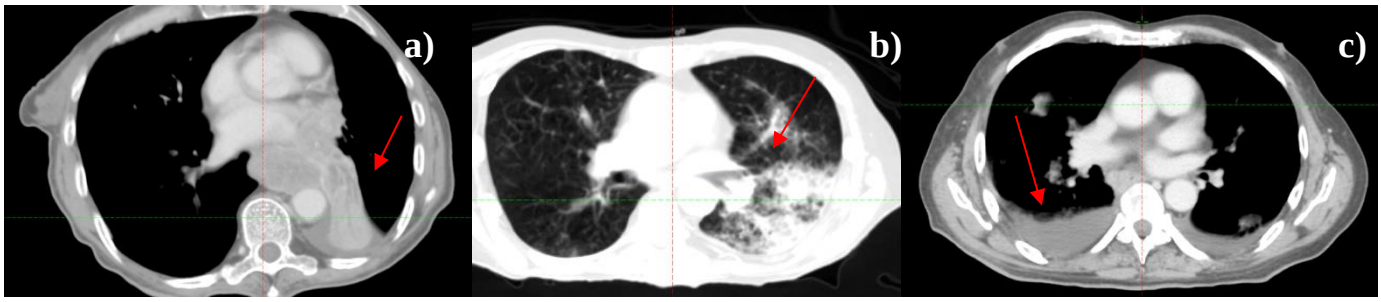

Figure 4: a) Atelectasis (red arrow) in thorax in a CT image, b) Pneumonitis (red arrow) in the lung lobe and c) Pleural fluid in both lung lobe.

2.5 Gamma index analysis

Gamma index analysis evaluates and compares the measured and calculated dose distribution. The dose distribution comparison can be divided into high- and low-dose gradients. The acceptance criteria in the low-dose gradient region are based on the dose differences (DD) between the measured and calculated dose distribution disagreement. In the high-dose gradient region, assuming that the spatial extension area is sufficiently large, the distance-to-agreement (DTA) is applied in the acceptability of dose calculation. DTA is described by the distance between a data point in the measured dose distribution and the nearest point in the calculated dose distribution exhibiting the same dose. The dose differences and DTA are two criteria used to determine the dose distribution calculation quality. [42] There are two methods of DD calculation, a local and global gamma index analysis. The local gamma index analysis calculated the DD relative to the dose at each evaluated point, while the global gamma index analysis calculated the DD relative to the prescribed dose or the maximum dose. [43]

3. Material and method

3.1 Patients

Twenty lung cancer patients with different treatment plans (NSCLC n = 14, SCLC n = 5, SBRT n = 1) were treated with conventional and stereotactic RT on Truebeam (Varian Medical Systems) and were selected for the project. The collected patient data was between 15 January 2018 and 15 December 2022 for patients with re-scanning CT due to anatomical changes. The observed anatomical changes were atelectasis (Ate, n = 5), tumor shrinkage (TS, n = 8), tumor positional deviation (TPD, n = 5), tumor enlargement (n=1), tumor dispersion (n=1), pleural effusion (PL), or pneumonitis (Pne), where 3 out of 6 TPD patients had pneumonitis, pleural effusion, or tumor shrinkage (Table 4, *Appendix A : Patient information*).

Among twenty patients, four NSCLC patients were treated with the DIBH technique, and the rest were treated with the FB technique. Most NSCLC patients received 66 Gy (33 fractions / 2 Gy per fraction), but two patients were treated according to the NARLAL2 clinical trial.[44–46] These patients were treated with a dose-escalated treatment plan with an inhomogeneous dose distribution, with dose-escalation within the target, driven by the FDG-avid volume. Here the mean dose to this escalation-volume for the primary and lymph node targets are allowed up to 95 Gy for GV_{PET-T} and 74 Gy for GTV_{PET-N} where the dose constraints for the OARs were limiting the maximum dose received. The five SCLC patients received 45 Gy (30 fraction/1.5 Gy per fraction, 2 fractions/day) or 50 Gy (25 fraction/ 2 Gy per fraction), and one SBRT patient had a prescribed dose of 67.5 Gy to the GTV (where PTV was covered by 45 Gy) in 3 fractions.

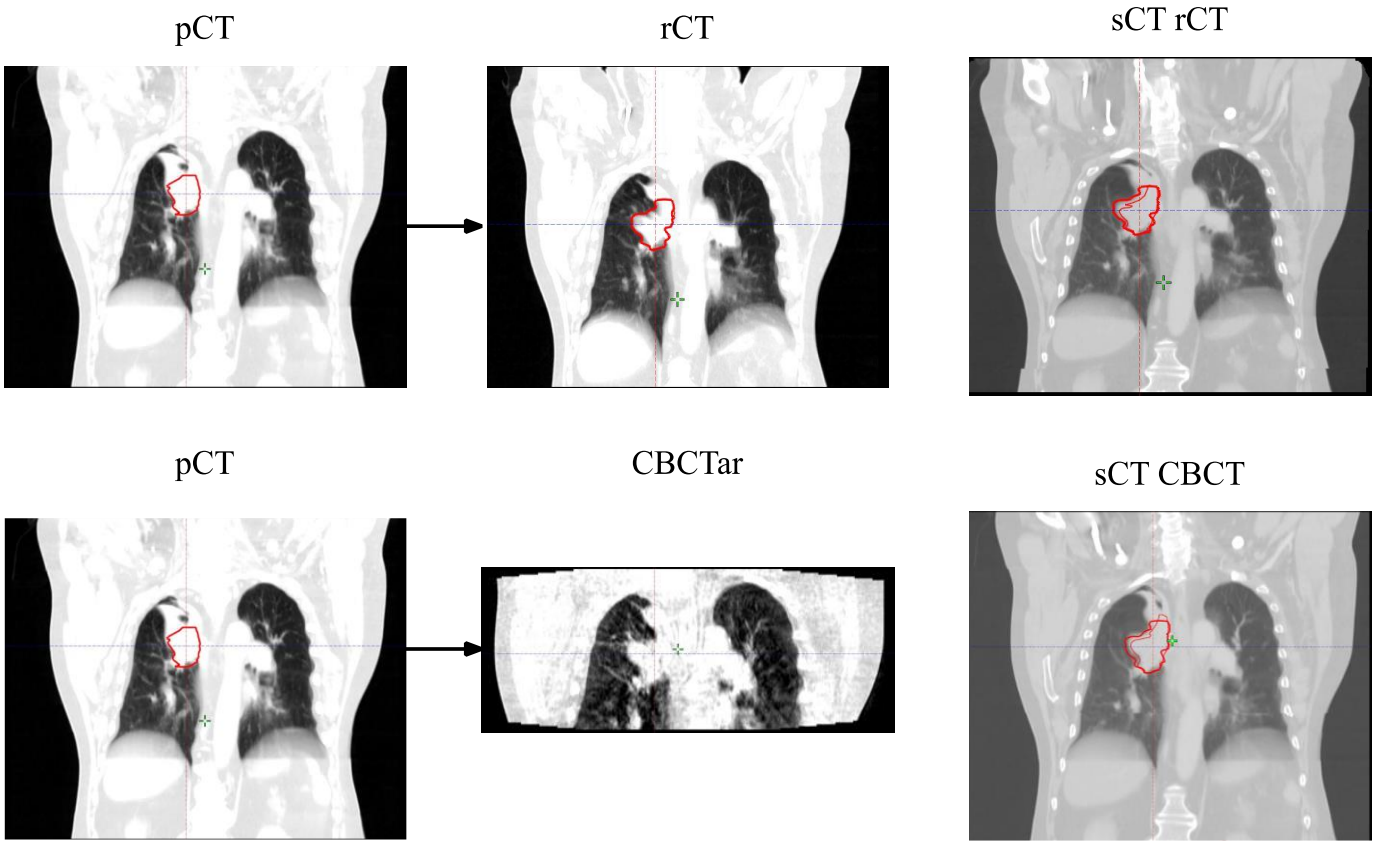

Figure 5: sCT generated by deforming pCT to rCT (row above) and CBCT (row below) of the new anatomy. Note the bold delineated GTV in sCTs image are structure transferred from rCT and the thinner line of GTV are the deformed structures generated in batch mode.

3.2 Phase 1: Generating sCT and dose calculation.

The original pCT, rCT, and the first CBCT post-re-planning images were acquired for each 20 patients to generate sCTs. sCTs images were generated in an Ethos emulator running in batch mode by Varian Medical Systems, where the pCT was deformed to rCT and CBCT post-re-planning CT to generate sCT_{rCT} and sCT_{CBCT}, respectively (Figure 5).

3.2.1 Dose calculation on sCT_{rCT}, sCT_{CBCT}, and CBCT

The relevant images had to be registered to the rCT in the dose calculation process. sCT_{rCT} and rCT were in the same frame of reference, and sCT_{CBCT} and CBCT were in the same frame of reference (Figure 6). Since this project was a retrospective study and acquiring rCT and CBCT images was impossible on the same day (images were taken 1-5 days apart, Table 4, *Appendix A : Patient information*), the geometrical information would differ. Therefore, the CBCT and rCT images had to be manually registered using auto-match using the Image registration module in Eclipse to compensate. The images were rigidly registered according to the clinical practice for online soft-tissue tumor match for lung cancer patients at Herlev Hospital. Registration was based on soft tissue registration on the GTV-T/IM (in FB) or GTV-T (in DIBH) structure with a margin of 1 cm, using an intensity range of [-1000; 250] HU. (Figure 7)

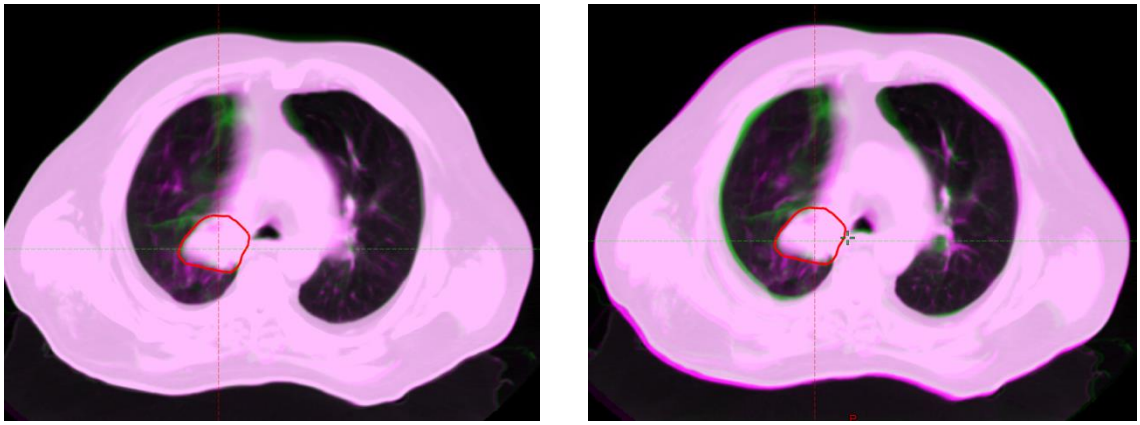

Figure 6: The rCT (green) and sCT_{rCT} (magenta) in the same frame of reference (left picture), and rCT (green) and sCT_{CBCT} (magenta) with image registration on target (right) for patient 1.

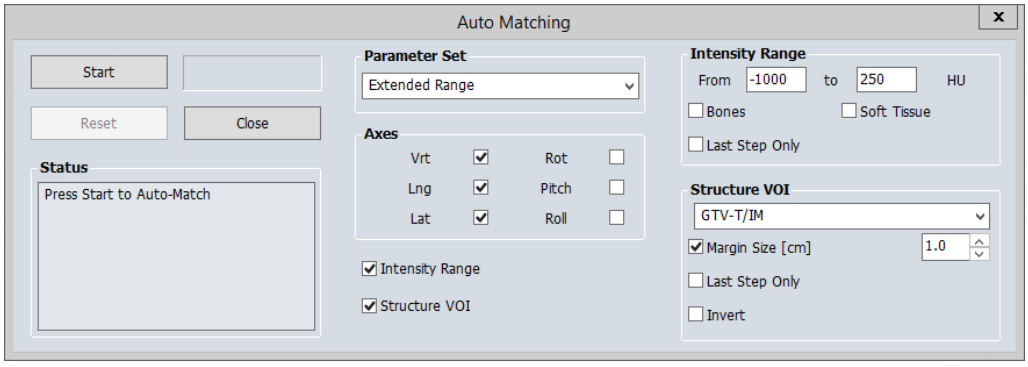

Figure 7: Soft tissue auto match settings for image registration between rCT and CBCT.

The main goal was to evaluate the dose calculation on the sCTs and compare the DVH data with the ground truth, the rCT, for each patient by performing a re-calculation without re-optimization. The original structure set and treatment plan from rCT were copied and transferred to sCT_{rCT} and sCT_{CBCT}, creating identical treatment plans. The imported structure set included the clinical target volume (CTV),

gross tumor volume (GTV), planning target volume (PTV), heart, lungs, esophagus, and spinal cord, and body structure generated from sCTs was kept.

The rCT treatment plan was additionally copied and transferred to the CBCT image, and a dose calculation was performed (dCBCT). In summary, re-calculations were performed for three treatment plans per patient (one treatment plan for sCT_{rCT}, one for sCT_{CBCT}, and one on CBCT) using Eclipse TPS v16.01.10 (Varian Medical Systems) with Anisotropic Analytical Algorithm (AAA) v.16.1.0 and the preset number of monitor units (MUs) from the rCT treatment plan. A different version of AAA (v. v.15.6.05) was applied for three patients due to older treatment plan data, and for the SBRT patients, the dose calculation algorithm was Acuros XB v.16.1.0.

3.2.2 Qualitative Observation on sCTs Image

The sCTs images generated from deforming pCT to rCT and CBCT were qualitatively evaluated using the image blend function in the Image Registration module in ARIA v.16.01.10, (Varian Medical Systems) in the lung window level and evaluated by the author. Anatomical differences in the images were noted to be **moderate** anatomical differences, indicating that the sCT is not close to rCT nor pCT (Figure 9), and **small** anatomical differences indicate that the sCT is more similar to rCT than pCT by comparing the target and OAR(Figure 8).

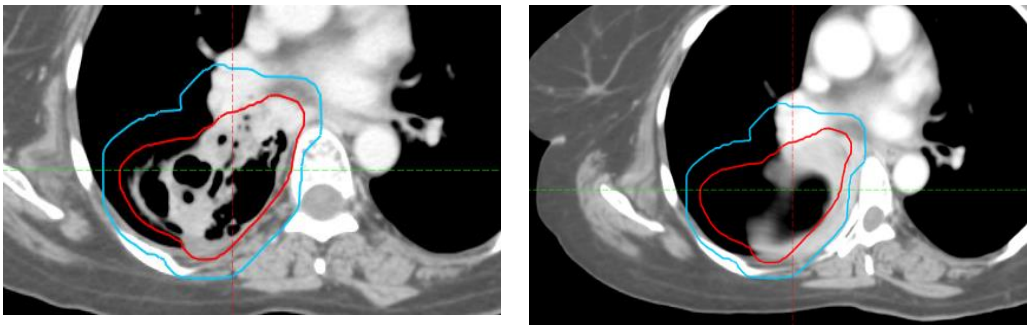

Figure 9: Example of moderate anatomical differences between rCT(left) and sCT_{rCT} (right) for patient 7. The window level as set in breast to visualize the spinal cord deformity.

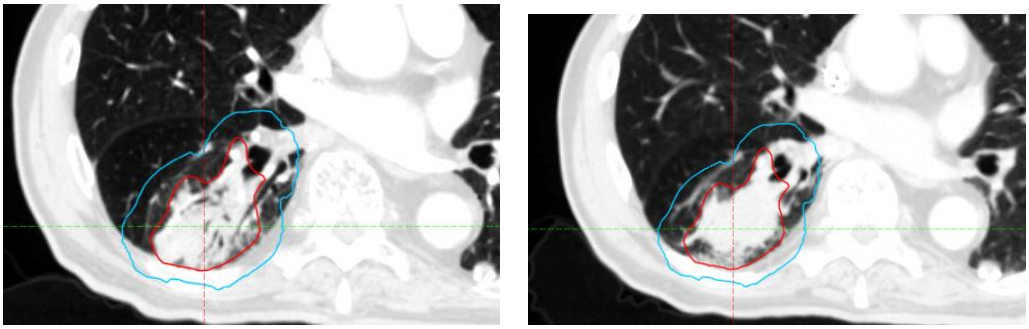

Figure 8: Example of small anatomical differences between rCT (left)and sCT_{rCT} (right) for patient 16, viewed in the lung window level.

3.2.3 Quantitatively Evaluation of Dose Calculation

In the evaluation process, a common ground had to be selected to compare the dose assessment between the treatment plan of rCT and the re-calculated plans with sCTs and dCBCT. Since patients in this project had different treatment methods and received different total radiation doses and number of fractions, the rCT was set to fulfill different clinical goals. A common ground was set for the dose of DVH analysis for structures such as GTV, PTV, spinal cord, total lung, heart, esophagus, and body (Table 1). The acceptable dose difference was set at 2%.

An in-house developed ESAPI script was used to extract the DVH dosimetry metrics from Eclipse TPS (Table 1).

Table 1: Dosimetry metrics for the targets and OAR structures with clinical constraints used to evaluate the treatment plans.

Structure	Target dose constraints	Clinical dose constraints
GTV	$D_{99\%}$	Dose to 99% of the GTV.
PTV	$D_{98\%}$	Dose to 98% of the PTV.
	$D_{2\%}$	Dose to 2% of the PTV (near maximum dose).
	D_{max}	Maximum dose of the PTV.
Structure	**OAR dose constraints**	**Clinical dose constraints**
Spinal cord	D_{max}	Maximum dose of the spinal cord.
Total lung	V_{5Gy}	Total lung volume that receives at least 5 Gy.
	V_{20Gy}	Total lung volume that receives at least 20 Gy.
	MLD	Mean lung dose (MLD)
Heart	V_{25Gy}	Heart volume that receives at least 25 Gy.
	V_{40Gy}	Heart volume that receives at least 40 Gy.
Esophagus	V_{55Gy}	Esophagus volume that receives at least 55 Gy.
	D_{mean}	Mean esophagus dose.
Body	D_{max}	Maximum dose of the body volume.

3.2.3.1 Statistics

Wilcoxon signed-rank test was used to compare the median value of rCT with sCT_{rCT}, $sCT_{CBCT,}$ and dCBCT, respectively, for each DVH parameter (Table 1). The nature of the data was not a normal distribution; therefore, a non-parametric test was chosen. The same patient population was used for all treatment plans, and the testing was based on paired data. The two-sided test with a significance level (α) was set to 0.05, and statistical analysis was performed in Matlab (Matlab R2020b) with the signrank function.

The null hypothesis $\mathbf{H_0}$ states that there are **no** median differences between the dose distribution of the rCT treatment plan and a similar treatment plan with sCTs or dCBCT.

The alternative hypothesis $\mathbf{H_1}$ states that there is **a median** difference between the dose distribution of the rCT treatment plan and a similar treatment plan with sCTs or dCBCT.

The differences in absorbed dose for the different structures were compared as the differences in rCT-sCT_{rCT}, rCT-sCT_{CBCT}, and rCT-dCBCT for each patient. Four patients were excluded from the sCT_{CBCT} and CBCT statistical analysis due to new or additional anatomical changes after re-scanning, discovered only afterward on the CBCT and the subsequent treatment fractions. The CBCT anatomy was, therefore, not similar to rCT and had to be excluded to avoid statistical uncertainties. The excluded patients were

3, 5, 10, and 13 (Figure 10, Table 4). Patient 3 was re-scanned due to the resolution of atelectasis; however, three days after re-scanning, the acquired CBCT displayed the re-appearance of the atelectasis (A in Figure 10, CBCT image in magenta demonstrates atelectasis while rCT in green with a resolution of atelectasis). Patients 5, 10, and 13 were re-scanned due to tumor positional deviation after re-scanning. The daily acquired CBCTs revealed additional tumor positional shifts for patient 5 in the anterior direction (B in Figure 10). Patient 10 was re-scanned due to tumor positional deviation and pneumonitis, and patient 13 was re-scanned due to tumor positional deviation, pleural effusion, and pneumonitis. The primary tumor on the thorax wall for both patients shifted in the caudal direction (C-D, in Figure 10). The tumor shift for patient 10 (Figure 10, C)is slightly more difficult to visualize due to pneumonitis.

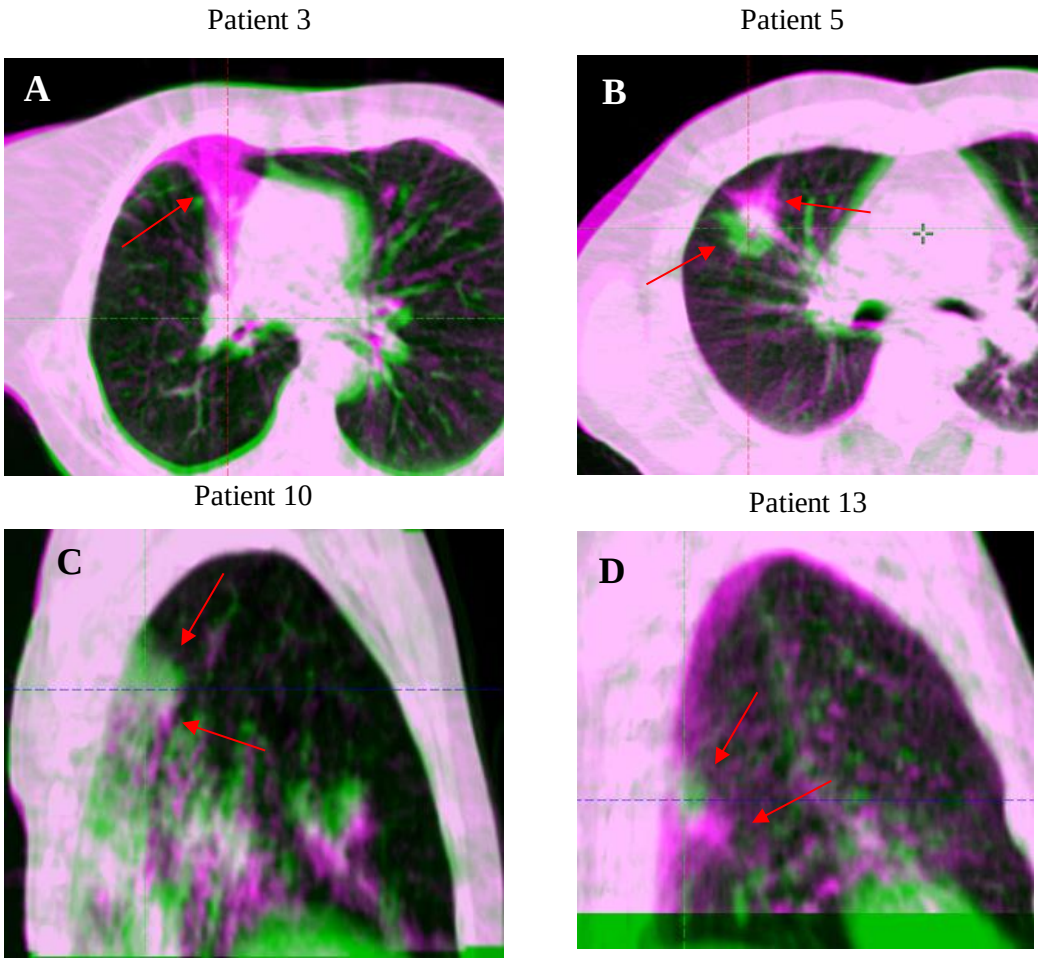

Figure 10: (A) Patient 3 with re-appearance of atelectasis on the first CBCT post-rCT, (B-D) tumor positional deviation on CBCT post-rCT for patients 5,10 and 13. In patients 10 and 13 the tumor shift was in the caudal direction for the CBCT. The image registration between CBCT and rCT (B-D) was according to bone ([50; 3000] HU) to highlight the tumor shift. (A-B) Images are in the transversal view and (C-D) in the sagittal view, with lung window level. In the blended images, rCT images are green, and CBCT is magenta; the red arrows highlight the anatomical change between rCT and CBCT.

3.3 Phase 2: Gamma index analysis

Gamma index analysis is performed using the freeware 3D Slicer image computing platform v.4.11 (www.slicer.org) to compare the dose distribution of the rCT with sCTs and dCBCT. Slicer is a software program to perform analysis, registration, interactive segmentation, and visualization of medical images. rCT, CBCT, sCT_{rCT}, and sCT_{CBCT} images, the corresponding dose distributions, and image registrations were exported from Eclipse TPS. The image registration done in the Eclipse Image registration module was used to register the dose distributions between rCT and CBCT/sCT_{CBCT} since they were not in the same frame of reference, as described earlier in section 3.2.1.

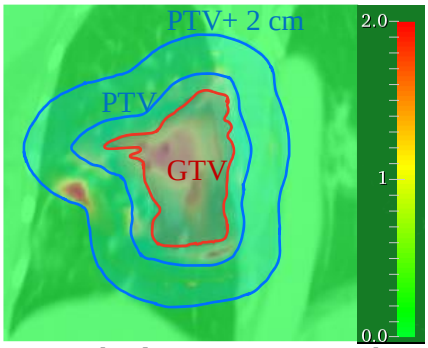

Figure 11: Absolut gamma map with GTV with red outline, PTV and PTV + 2 cm margin contour with blue outline. The color bar displays the gamma value, where gamma value > 1 indicate that the criteria failed.

The input-to-dose comparison in 3D Slicer required a dose distribution of a reference dose volume (rCT) and the evaluated dose volume (sCT_{rCT}, sCT_{CBCT}, dCBCT). The criteria for performing gamma index analysis were local gamma with 2%/2 mm and 20% threshold of the maximum dose. Gamma rate analysis was evaluated within the PTV + 2 cm margin structure and cropped to the body structure of the CBCT (Figure 11). The output was the passing rate fraction and absolute gamma map of the region where the criteria passed or failed. Any gamma value <1 indicates a passing gamma criterion and is highlighted in green, and a gamma value > 1 illustrated with warmer colors such as yellow, orange, and red for region indicates areas that failed the gamma criteria (Figure 11). Despite only performing gamma index analysis inside PTV + 2cm, the gamma map in 3D Slicer will automatically highlight the outside calculated structure with green (Figure 11).

4. Result

4.1 sCT image evaluation

The generated sCT generally displayed promising anatomical replication from deforming pCT to rCT and CBCT, respectively. Overall, 12 out of 20 sCT_{rCT} patients had an anatomical disagreement between rCT and sCT (9 out of 12 were evaluated to have a moderate anatomical disagreement, and 3 out of 12 had a small anatomical disagreement), and 14 out of 20 sCT_{CBCT} displayed anatomical disagreement (11 out of 14 had a moderate anatomical difference, and 3 out of 14 had small anatomical differences). The rCT image was set as the ground truth.

Patients 6, 7, 8, 9, 10, 12, 13, 15, and 17 had moderate anatomical differences between rCT and sCT, and patients 14,16 and 18 had a small anatomical difference between rCT and sCT. The additional two patients (patients 3 and 5) for sCT_{CBCT} were due to anatomical changes between rCT and CBCT.

This section will present pCT, rCT, CBCT, and sCTs for some patients. A general observation was that the sCT tended to carry some specific characteristic from the pCT despite not existing in rCT or CBCT. Only a few of the same types of anatomical disagreement will be presented in this section, and the rest is found in *Appendix B: Patient images*.

Patients 6, 7, and 17 were re-scanned due to TS (*4.1.1 Patient examples: Re-scanned due to tumor* shrinkage), and patients 3, 10, and 13 were the patients excluded from the statistical analysis of sCT_{CBCT} due to the large anatomical disagreement between CBCT and rCT (*4.1.2 Patients excluded from statistical analyses due to large anatomical changes in sCTCBCT).*

4.1.1 Patient examples: Re-scanned due to tumor shrinkage

Patient 6 was re-scanned due to tumor shrinkage (Figure 12). The tumor shrinkage was observed when comparing the rCT to the pCT. The corresponding sCTs were deformed from pCT to rCT and CBCT, simulating that volume change. However, in the center of the target, the sCTs (red arrows) were more homogenous in contrast to the rCT and CBCT images (green arrows). Some tissue at the center of the target in the original pCT disappeared during the course of treatment, where holes were observed in rCT and CBCT but not replicated correctly in the resulting sCTs.

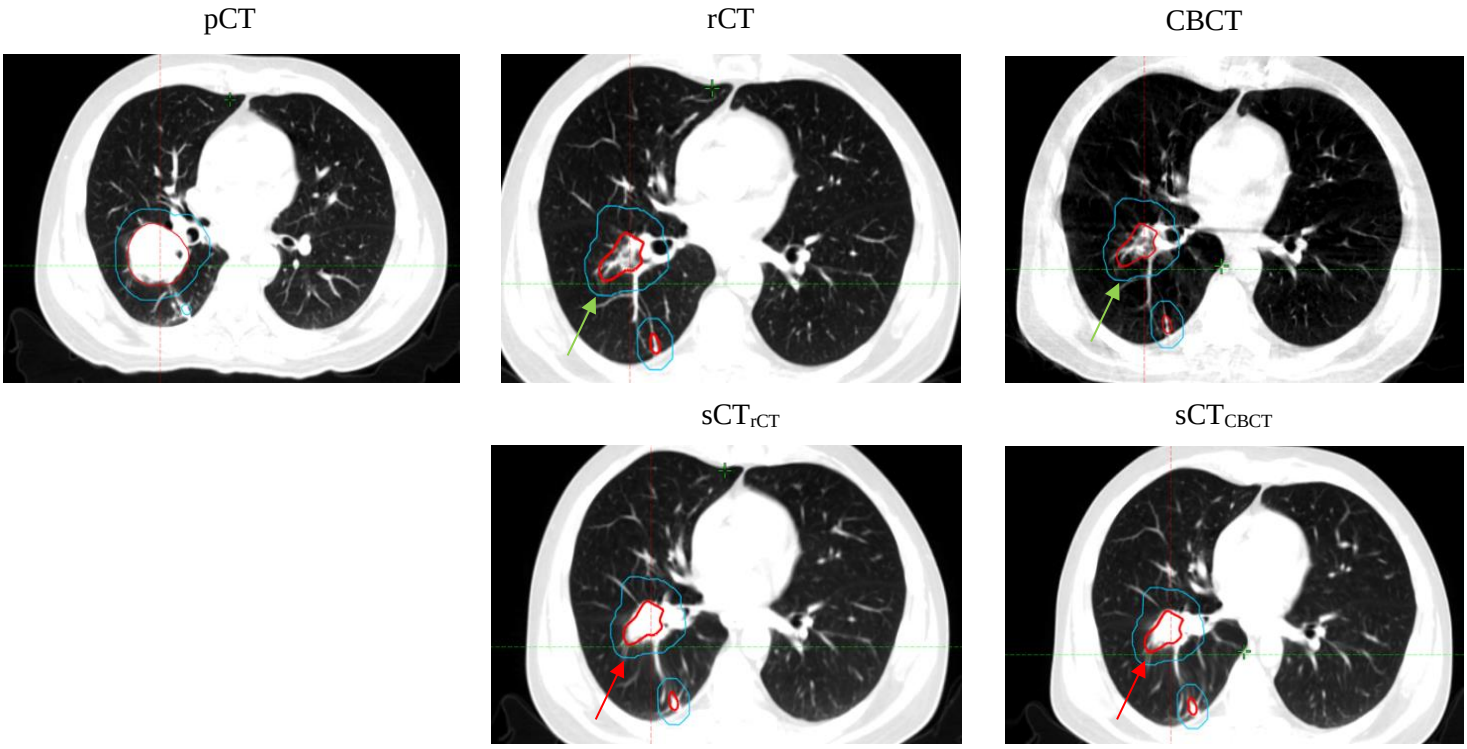

Figure 12: Patient 6 was re-scanned due to tumor shrinkage. Images are presented in transversal view with lung window level, where GTV (red) and PTV (blue) structures presented are propagated from the rCT (considered as the ground truth structures). Tumor shrinkage was observed in both the sCT_{rCT} and sCT_{CBCT} images. However, the soft tissue disappearing centrally in the tumor during the course of treatment was not replicated correctly. The red arrows highlight the homogenous area in the sCT compared to rCT and CBCT images highlighted with green arrows.

Patient 7 experienced tumor dispersion (Figure 13). The resulting sCTs had more difficulty replicating the anatomical change than patient 6 (Figure 12). The anatomical change was not correctly deformed and resulted in unrealistic sCTs (and sCT_{CBCT}), affecting the shape of the spine, and resulting in the erroneous shape of the target volume, missing some lateral part on the right side of the tumor, and highlighted with red arrows.

Patient 17 was re-scanned due to tumor shrinkage (Figure 14). The target in pCT had a characteristic shape (visible within the green square). This shape was present in the sCTs despite not existing in the rCT and CBCT (highlighted with red and green squares in Figure 14)). Nevertheless, the shrinkage of the target in rCT and CBCT was somewhat replicated in the sCTs. This patient set an excellent example of anatomical change, which caused the sCT to have some distinct characteristic mixture from pCT and rCT/ CBCT.

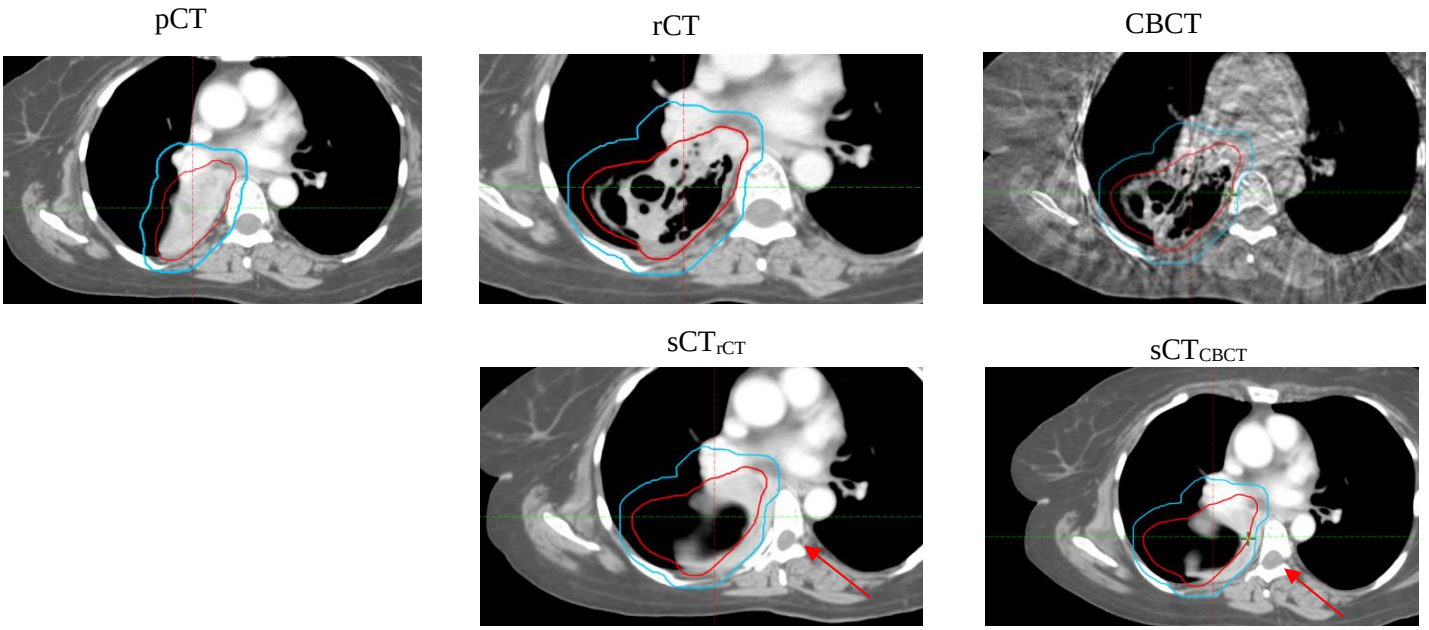

Figure 13: Patient 7 re-scanned due to tissue dispersion. Images are presented in transversal view with "breast" window level to illustrate the spinal cord deformity. The GTV (red) and PTV (blue) structures presented are propagated from the rCT (considered as the ground truth structures), except from pCT image where the structure is propagated from pCT. The target was shifted into the spine and caused an unrealistic deformity (red arrows).

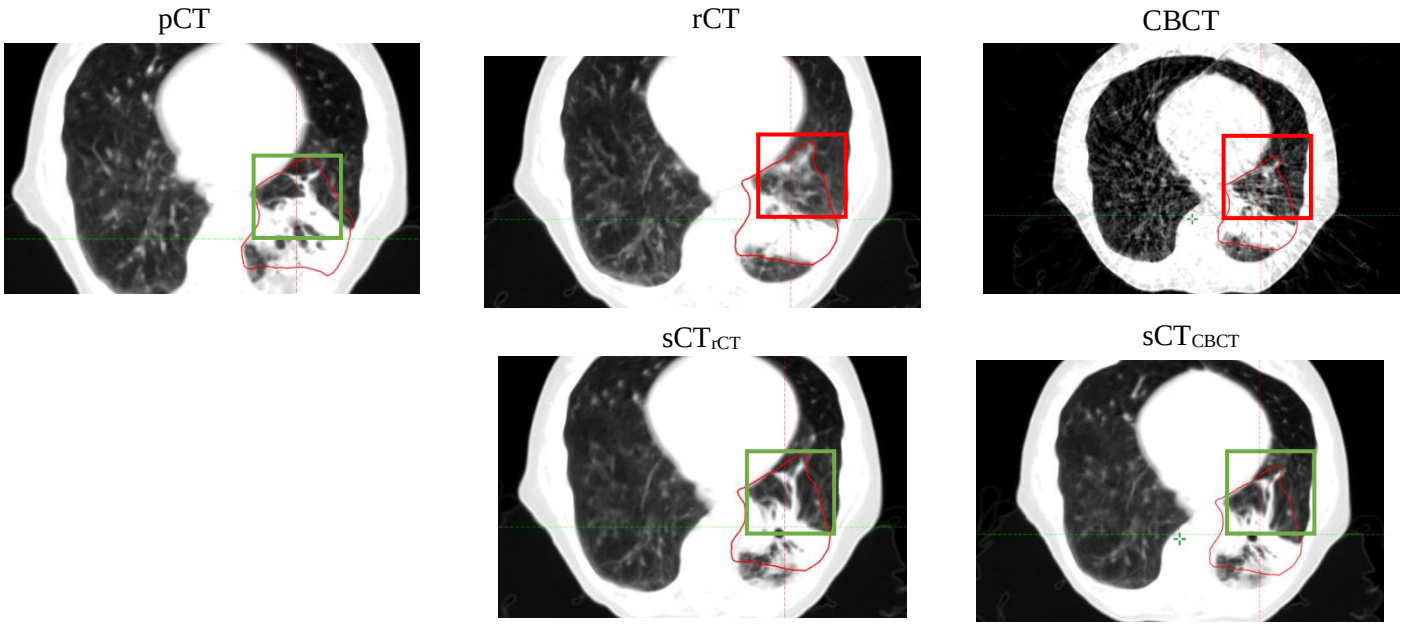

Figure 14: Patient 17 re-scanned due to tumor shrinkage. Images are presented in transversal view, and lung window level where GTV (red) structures presented are propagated from the rCT (considered as the ground truth structure), except for pCT image where GTV structure are propagated from pCT. The characteristic shape visible in the pCT is also present in the sCT images, apparent within the green square. Resulting sCTs have characteristics that are a mixture of pCT and rCT/CBCT features.

4.1.2 Patients excluded from statistical analyses due to large anatomical changes in sCT_{CBCT}

The following sets of patients are 3 out of 4 patients who were excluded from the statistical analysis for sCT_{CBCT}.

Patient 3 had atelectasis during the simulation and at treatment start, observed on the pCT and CBCT, which shifted the whole mediastinum area to the right side of the thorax (A, red arrow). The patient was re-scanned due to atelectasis resolution some fractions later (B, green arrow). After re-planning, in the CBCT (acquired three days after re-planning), the atelectasis appeared in the exact location as during simulation (C-D). In the case where atelectasis re-appeared during treatment at the same location as observed during simulation, the resulting sCT_{CBCT} agreed well with the pCT since that anatomical change already existed in the pCT, used for deformation. The patient was excluded from the sCT_{CBCT} statistical analysis because of the anatomical disagreement between sCT_{CBCT} and sCT_{rCT} since rCT was obtained during the period where the atelectasis was resolved.

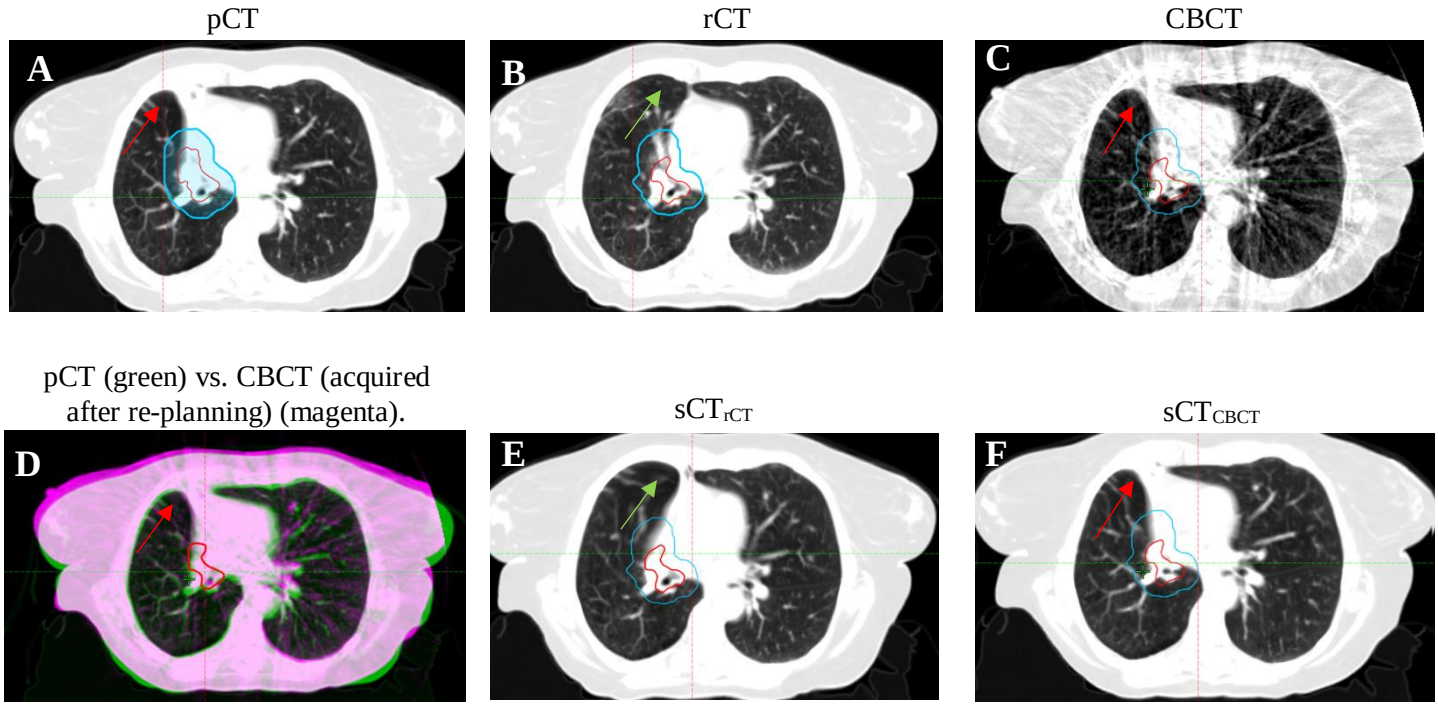

Figure 15: Patient 3 had appearance and resolvent of atelectasis during the course of treatment. The relevant images are presented here in the transversal view with lung window level. (B-F) The GTV (red) and PTV (blue) structures are propagated from rCT (considered as the ground truth structure), (A) The GTV and PTV structure are propagated from pCT. (A) atelectasis was present at pCT highlighted with red arrows, which shifted the mediastinum to the right side of the thorax. (B) rCT, where atelectasis had resolved(green arrow), and the mediastinum were located in its normal state. (C) CBCT (acquired after rCT was obtained), where the former atelectasis re-appeared in same location as during simulation and treatment start (D). (E) sCT_{rCT} correctly simulate resolved atelectasis and (F) correctly simulated the appearance of atelectasis.

Patient 10 was re-scanned due to tumor positional deviation and the appearance of pneumonitis (A-C, the white arrow was the tumor position at pCT, and the blue arrow highlighted the shift in position in rCT). The sCT_{rCT} had difficulty simulating the target and pneumonitis (since it did not exist in pCT) (D). The primary target close to the thoracic wall in sCT_{rCT} is not well defined and similar to the pCT target, and the pneumonitis is almost not visible in the sCT_{rCT} or sCT_{CBCT}. This patient was also excluded in the sCT_{CBCT} statistical analysis due to a large tumor positional shift (in the caudal direction) in the CBCT compared to the rCT (F), where the CBCT was acquired 2 days after rCT acquisition. This large

tumor shift and pneumonitis were not correctly handled by the deformation when generating the sCTs (D-E, G-H

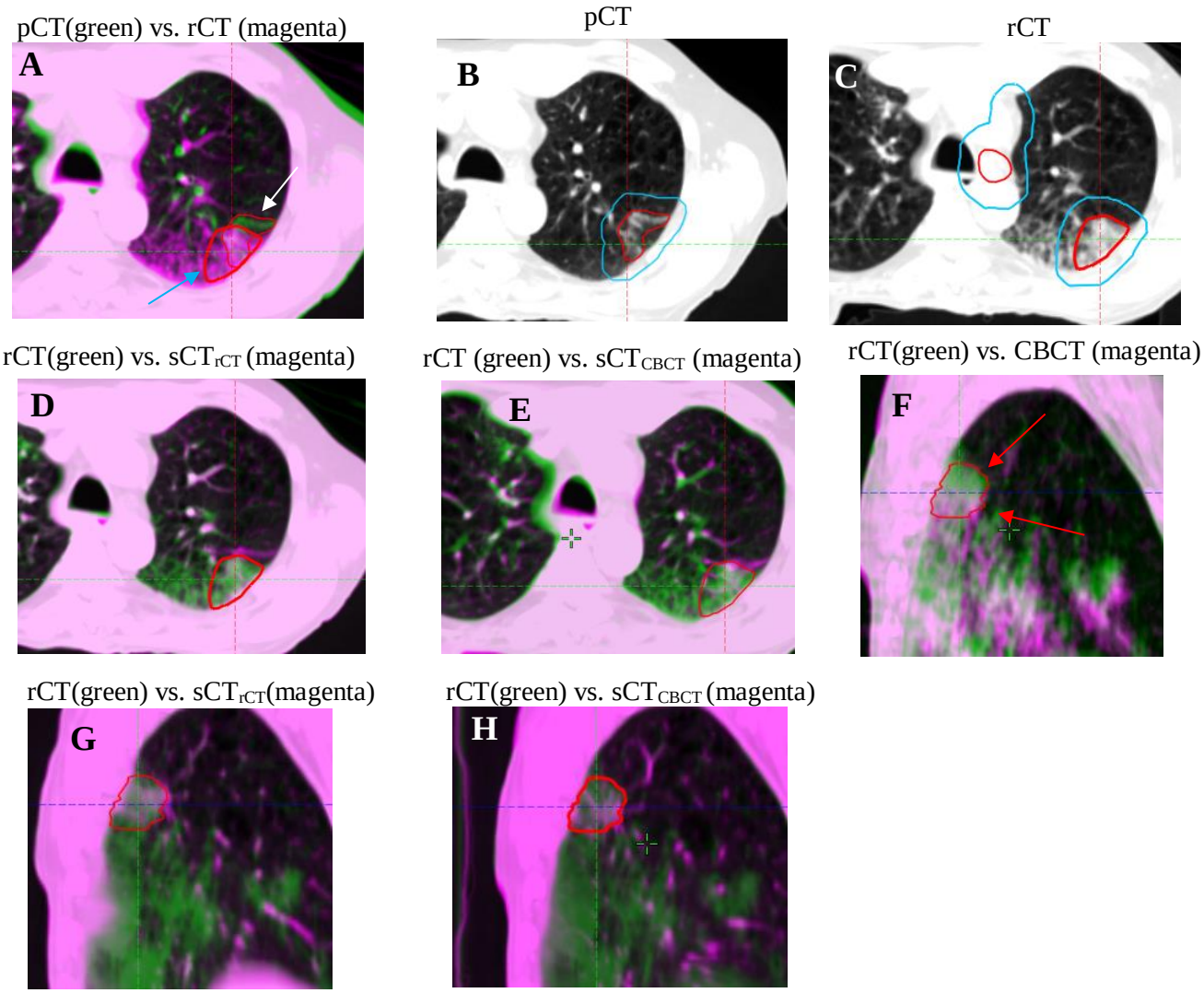

Figure 16: Patient 10 re-scanned due to large shift of tumor position and pneumonitis. Images are presented in transversal (A-E) and sagittal view (F-H) in lung window level. (C-H) The GTV (red) and PTV (blue) structures presented are propagated from the rCT (considered as the ground truth structures), the bold GTV and PTV structure (A ,B) are propagated to the original pCT (the white arrow highlight tumor position in pCT and blue arrow highlight the shift in rCT). The tumor located close to the left side of the thoracic wall is not easily defined in the sCT_{rCT} or sCT_{CBCT} images (D-E). The blended image of rCT vs. sCT_{rCT} and rCT vs. sCT_{CBCT} (D-E,G-H) clearly visualizes that the pneumonitis is not correctly taken into account during the generation of sCT_{rCT}. In the sagittal view (F) a tumor shift in the caudal direction is displayed, tumor in rCT and CBCT are highlighted with red arrows.

Patient 13 was re-scanned due to tumor positional deviation (applied for GTV-T), tumor shrinkage (applied for GTV-N), pleural effusion (blue arrow in Figure 17, A), and pneumonitis (green square in, A) in the right lung. Figure 17(A-D) illustrates the anatomical change of tumor shift for GTV-T, pneumonitis, and pleural effusion by blended images in the transversal view. The tumor position deviation between pCT and rCT image acquisition is highlighted with a red square (Figure 17, A). Figure 17(E-G) illustrates the corresponding blended images for the tumor shrinkage observed for GTV-N (red square in Figure 17, E). The positional shift of the primary tumor was observed in the CBCT compared to the rCT (Figure 17, H), where the CBCT was acquired 4 days after rCT acquisition. As a result of the

large tumor shift, pneumonitis, and pleural effusion that was not corrected correctly by deformation in sCT_{CBCT}, the patient was excluded from the sCT_{CBCT} statical analysis.

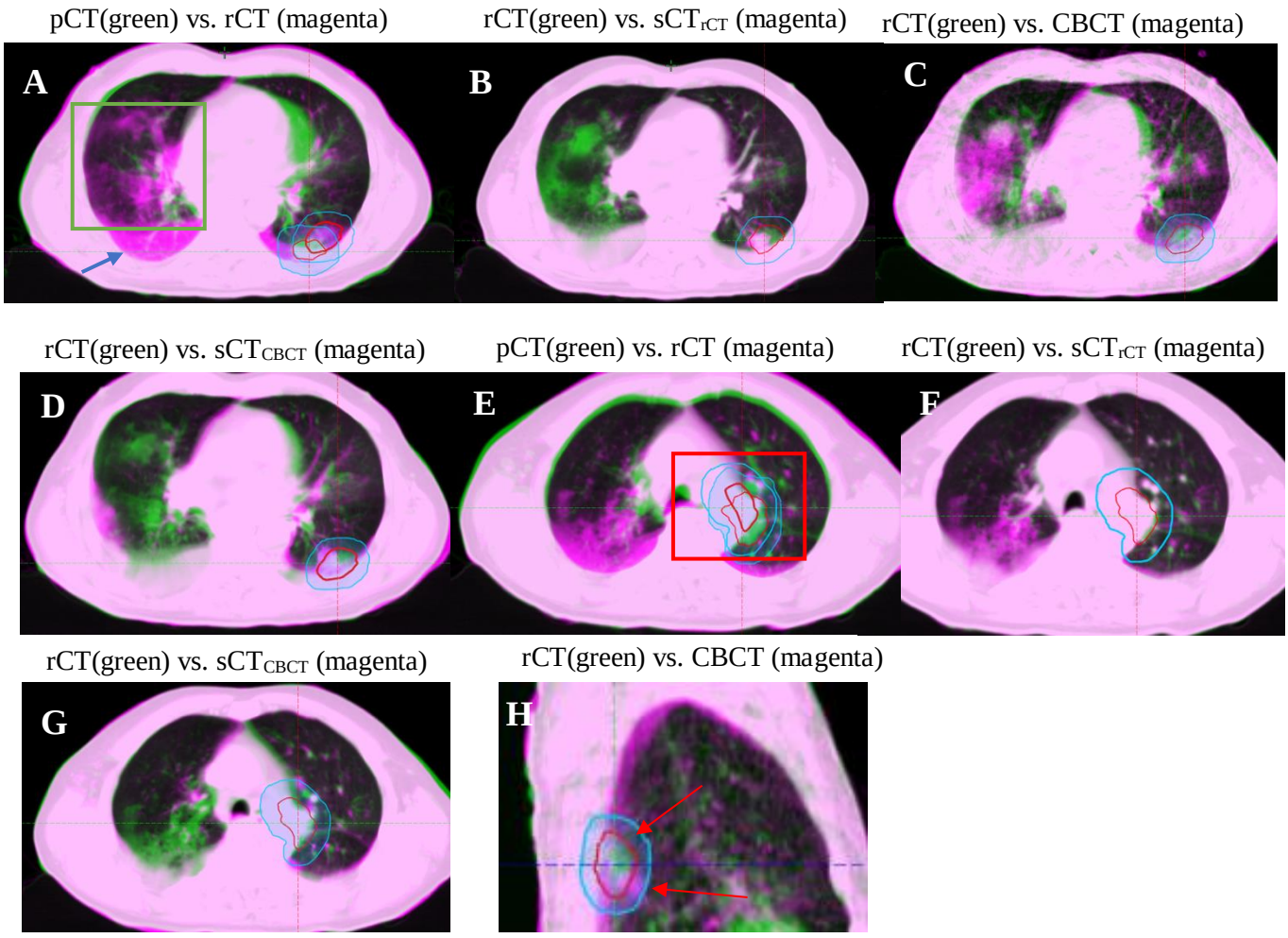

Figure 17: Patient 13 re-scanned due to tumor positional deviation (applied for GTV-T, visible in (A-D), tumor shrinkage (applied for GTV-N, visible in E-G and highlighted in red square), pleural effusion (blue arrow in A) and pneumonitis (green square in A) in the right lung. Images are presented in transversal view, (B-D,F-H) where GTV (red) and PTV (blue) structures presented are propagated from the rCT (considered as the ground truth structures) except for A and H image with structure from pCT.(A, H) PTV and GTV structure in bold belong to the original pCT. The anatomical changes were not able to be corrected for correctly by deformation when generating the sCTs (B,D). (H) The tumor positional deviation in the caudal direction was discovered in the first CBCT post-rCT (red arrows).

4.2 Dose distribution comparison between rCT and sCTs plan

4.2.1 Statistical analysis for between rCT and sCTs

The median differences for structure PTV with dose constraints $D_{98\%}$, $D_{2\%}$, and D_{max} and Body D_{max} were statically significant between rCT and sCT_{rCT} (n = 20) (Table 2). In addition, when comparing rCT with sCT_{CBCT} (n = 16), there was a statically significant median difference for $D_{99\%}$ of GTV volume. However, no statistically significant median differences were found for the OAR structures evaluated.

A negative median value indicated a higher absorbed dose in the sCTs plan than the rCT plan, and a positive median value indicated a higher absorbed dose in rCT than sCTs. Structures such as PTV $D_{2\%}$, PTV $D_{max,}$ and BODY D_{max} resulted in higher doses in the re-calculated sCTs plans.

The median dose differences for rCT- sCT_{CBCT} are lower for PTV D_{max} and body $D_{max;\ however}$ higher for GTV $D_{99\%}$ and PTV $D_{98\%}$ in contrast to rCT-$sCT_{rCT.}$ For rCT-$sCT_{rCT,}$ the median difference is less than 0.5 % and 1.3 % for rCT-sCT_{rCT} and rCT-sCT_{CBCT}, respectively. The median differences were within the acceptable 2% dose differences.

Table 2: Median, minimum, and maximum dose difference with a p-value for GTV, PTV, spinal cord, lungs, heart, esophagus, and body. Bold values indicate statistically significant median differences evaluated by Wilcoxon sign rank testing, where $\alpha = 0.05$.

	n= 20 Median [min; max]% (p-value)	n =16 Median [min; max]% (p-value)
DVH dose constraints	**rCT-sCT_{rCT}**	**rCT-sCT_{CBCT}**
GTV $D_{99\%}$	0.3 [-2.0; 4.0] (0.073)	**0.6 [-0.8; 3.8] (0.020)**
PTV $D_{98\%}$	**0.3[-0.2; 3.4] (0.001)**	**0.5 [-0.1; 3.2] (0.001)**
PTV $D_{2\%}$	**-0.2[-4.4;0.7] (0.014)**	**-0.2 [-3.6; 1.0] (0.017)**
PTV D_{max}	**-0.4 [-7.3; 0.9]** (**0.023)**	**-1.3[-9.0; 1.4] (0.017)**
Spinal cord D_{max}	0.0 [-1.1; 0.5] (0.911)	0.0 [-2.1; 0.9] (0.796
Lung V_{5Gy}	0.0 [-1.4; 0.9](0.296)	0.1[-1.4; 1.7] (0.877)
Lung V_{20Gy}	0.0[-0.5; 0.2] (0.332)	0.0 [-0.4; 1.0] (0.959)
MLD	0.0 [-0.2; 0.1](0.263)	0.0 [-0.2; 0.8] (0.756)
Heart V_{25Gy}	0.0 [-0.7; 1.0] (0.446)	0.0 [-0.6; 0.7] (1.000)
Heart V_{40Gy}	0.0 [-0.7; 0.6] (0.396)	0.0 [-1.1; 0.5] (0.561)
Esophagus V_{55Gy}	0.0 [-0.2; 0.5] (0.080)	0.0 [-2.3; 0.6] (0.700)
Esophagus D_{mean}	0.0 [-0.3; 0.2] (0.247)	0.0 [-0.8; 0.4] (0.717)
BODY D_{max}	**-0.4 [-7.2; 2.0] (0.023)**	**-1.0 [-8.1; 1.4] (0.023)**

n = number of patients

4.2.2 Dose distribution analysis of rCT and re-calculated sCTs and CBCT plan.

Data points for DVH metrics from two data sets and their agreement were visualized with an identity line plot for target GTV and PTV (Figure 18). The identity line plot compares different datasets, and if two data sets were equal, the data points would fall on the reference line (black line, which is the rCT data point).
The escalated plan for the two NARLAL patients and one SBRT patient resulted in deviating data points (Figure 18, A), which caused other data points to be challenging to evaluate. Therefore, some plots were zoomed in on PTV $D_{98\%}$, PTV $D_{2\%}$, and PTV D_{max} metric (Figure 18, B). For some patients, DVH target parameters for sCT_{rCT}, sCT_{CBCT}, and dCBCT demonstrated relatively good dose agreement with rCT, and the rest had a larger dose deviation. The reference line plot was conducted for the OAR, comparing the rCT DVH data with sCT_{rCT}, sCT_{CBCT}, and dCBCT, respectively (Figure 19). The sCT_{rCT} and sCT_{CBCT} had good dose agreement dose rCT. However, the dCBCT illustrates the higher dose for the total lung, heart, and esophagus.

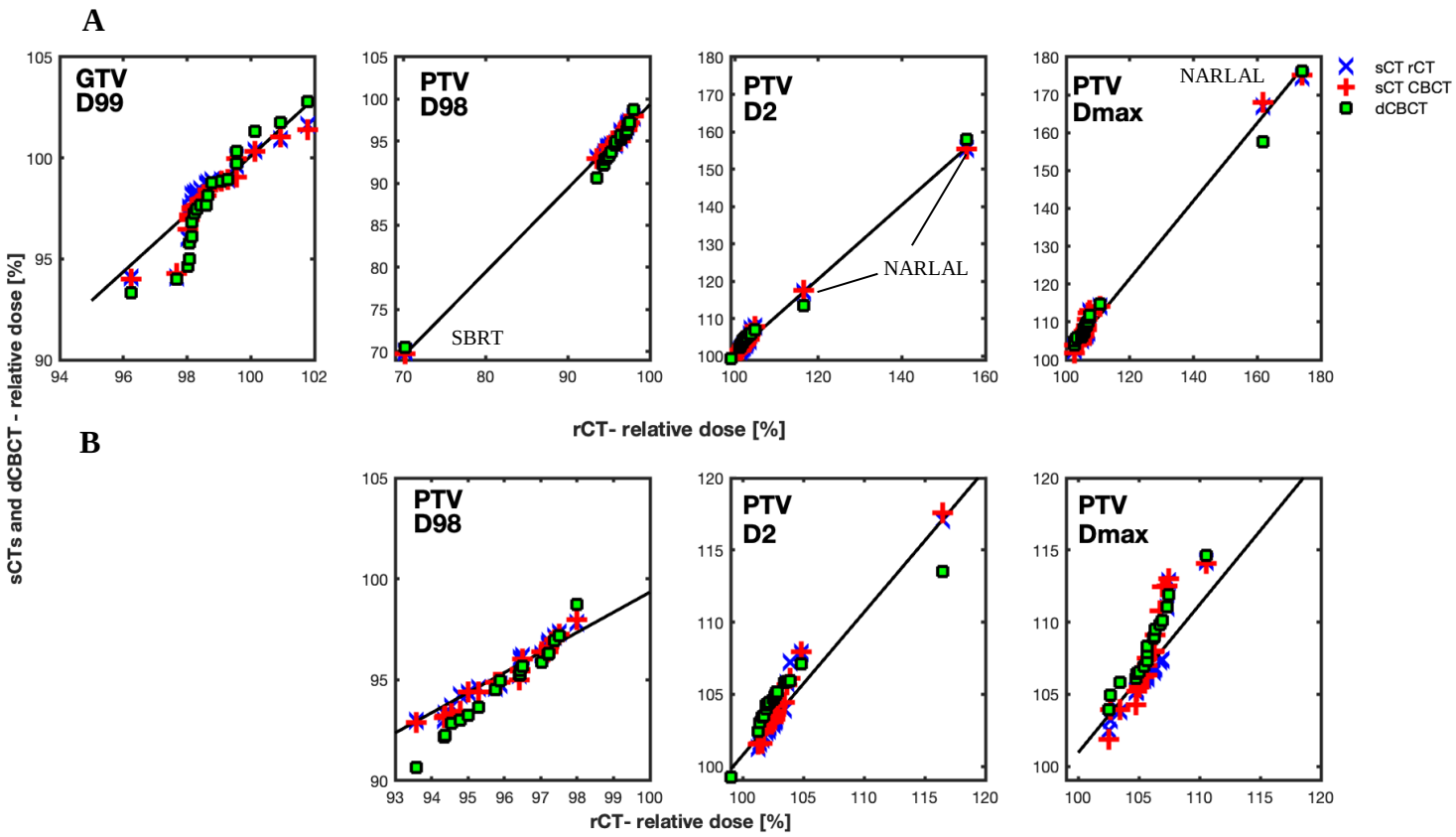

Figure 18: Data points with a reference line at evaluated DVH metrics for the target structures (n = 20). In the upper row, A, visualize the complete data set. In the lower row, B, are the zoomed in version of the DVH metrics from row A. The x-axis is the DVH metrics belonging to rCT, and the y-axis is sCT_{rCT} (blue X), sCT_{CBCT} (red cross), dCBCT (green square) DVH data points and black line is the reference line.

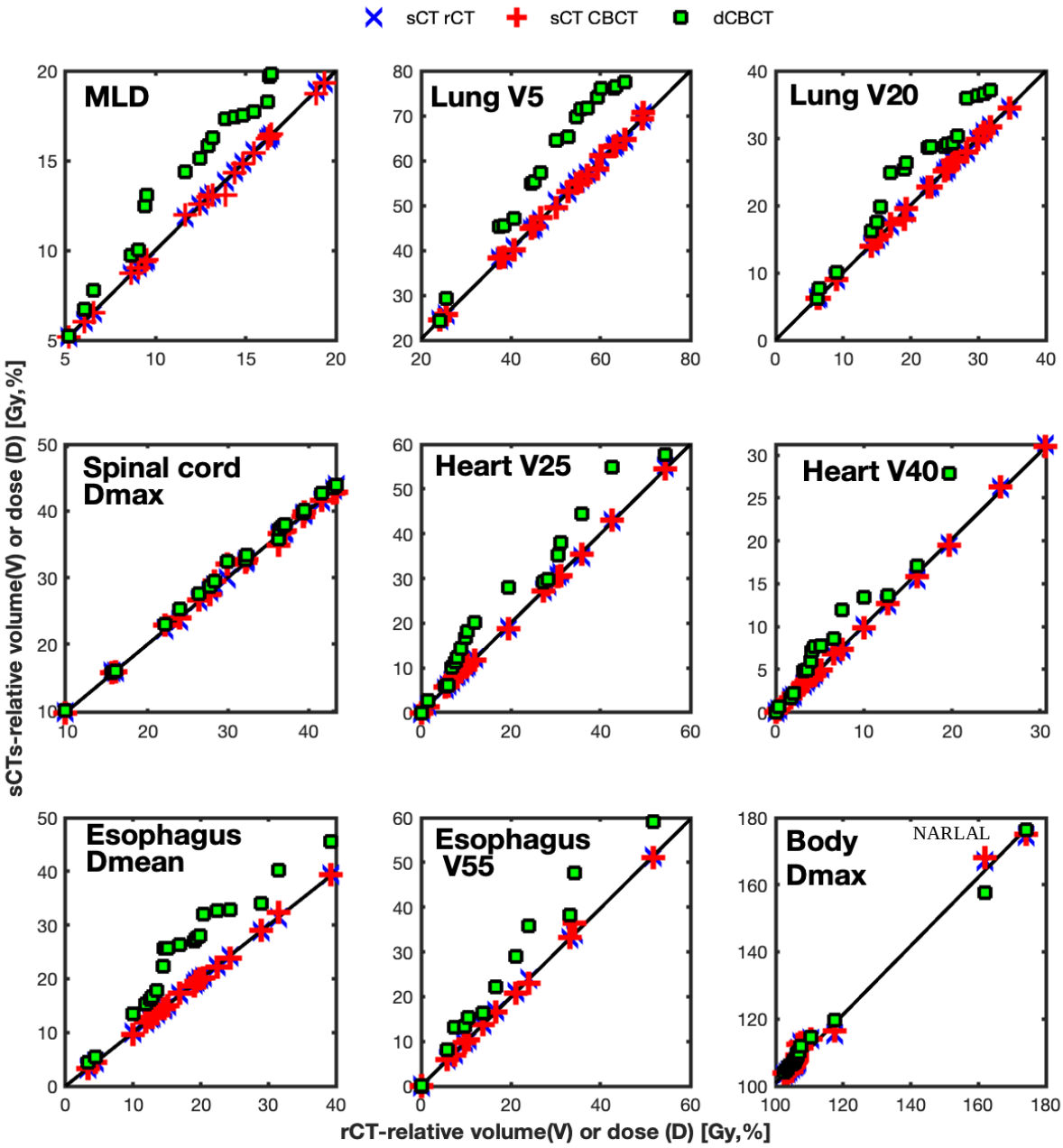

Figure 19: Data points with a reference line at evaluated DVH metrics for OAR structures (n = 20). In the upper row, A, visualize the complete data set. In the lower row, B, are the zoomed in version of the DVH metrics from row A. The x-axis is the DVH metrics belonging to rCT, and the y-axis is sCT_{rCT} (blue X), sCT_{CBCT} (red cross) and dCBCT (green square) DVH data points.

The absorbed dose difference from rCT- sCT_{rCT}, rCT- $sCT_{CBCT,}$ and rCT- dCBCT for every DVH parameter for the target and OAR was displayed with a boxplot (in Figure 20, respectively Figure 21). A boxplot describes the minimum, first quartile, median, third quartile, and maximum. The first quartile to the third quartile is defined by the box, the vertical line in the middle of the box is the median value, and the whiskers (vertical line outside the box) define the minimum and maximum value of the dataset. [47]

The absorbed dose disagreement for rCT-dCBCT -1.6[-3.7; 5.1]%, -1.6[-3.7; 3.0]%, 1.1[-1.3; 5.1]% and -2.2[-5.7; 4.3]% for GTV $D_{99\%}$, PTV $D_{2\%}$,PTV $D_{98\%}$ and PTV D_{max}, respectively. The absorbed dose difference to OAR structures were -1.9[-6.8; -0.1]%, -8.0 [-35.5;-0.2], -4.0 [-11.5; -0.1]%,-7.2 [-15.2; 1.6]%, 1.9[-14.6; 0.1]%, -1.7 [-27.1; 7.6]%, -0.9 [-18.2; 3.5]%, -0.7[-7.4; 4.7]% and -2.2[-5.7; 4.3]% for MLD, Lung V_{5Gy}, Lung V_{20Gy}, esophagus D_{mean}, esophagus V_{55Gy} ,heart V_{25Gy}, heart V_{40Gy}, spinal cord D_{max} and body D_{max}, respectively.

The outliers in rCT- sCT_{rCT} were caused by the same set of patients: 6 (TS), 7 (TS), 10 (TPD and Pne), 14(TPD), 15(Ate), 18(TS), and 19 (TPD and TS). Outliers in rCT-sCT_{CBCT} in the target DVH parameters belonged to patients 6, 9 (TS), and 18. Furthermore, the outliers in rCT-dCBCT for the PTV $D_{2\%}$ and PTV D_{max} belonged to patients 6, 8(TS,) and OAR outliers in rCT-dCBCT belonged to patients 8 (TS), 19, and 20 (TS).

A list of the patients who caused the outlier values for any DVH parameter over 2.0% for rCT- sCT_{rCT} with an evaluation of the sCT_{rCT} and rCT image comparison:

- Patient 6: The dose difference was -3.7%, -7.8%, and -7.2% for PTV $D_{2\%}$ and PTV D_{max} and Body D_{max}, respectively. The anatomical differences between sCT_{rCT} and rCT were evaluated to have moderate differences.
- Patient 7: The dose difference for outliers was 2.2% for PTV$D_{98\%,}$ and the anatomical difference was evaluated to be moderate between rCT and sCT_{rCT}.
- Patient 10: The outlier dose difference was -2.0%, -4.4%, -5.6%, and -5.6% for GTV $D_{99\%}$, PTV $D_{2\%}$, PTV D_{max}, and body D_{max}, respectively. This patient had moderate anatomical differences between rCT and sCT_{rCT}.
- Patient 14: An outlier with a 2.2% dose difference for GTV $D_{99\%,}$ and this patient had small anatomical differences between rCT and sCT_{rCT}.
- Patient 15: The target outlier had -3.1% and -3.6% dose differences for PTV $D_{2\%}$ and PTV D_{max}. This patient had moderate anatomical differences between rCT and sCT_{rCT}.
- Patient 18: The target had a dose difference of 4.0% and 3.4% for GTV $D_{99\%}$ and PTV $D_{98\%}$, respectively. This patient had small anatomical differences between rCT and sCT_{rCT}.
- Patient 19: This patient had a dose difference of -5.0% (PTV Dmax: -5.0%). The patient had an anatomical agreement between rCT and sCT_{rCT}.

The outliers in rCT- sCT_{CBCT} were caused by:

- Patient 6: The dose difference was -3.6% and -9.0% for PTV $D_{2\%}$ and PTV D_{max}, respectively. For OAR, the dose difference was -2.1%, -2.3%, and -8.1% for spinal cord D_{max}, esophagus $V_{55Gy,}$ and body D_{max}, respectively. This patient had moderate anatomical differences between rCT and sCT_{CBCT}.
- Patient 18: The dose difference was 3.8% and 3.2% for GTV $D_{99\%}$ and PTV$D_{98\%}$. This patient had small anatomical differences between rCT and sCT_{CBCT}.

In summary, the outliers in rCT- sCT_{rCT}, rCT- sCT_{CBCT}, and rCT-dCBCT were caused by the same set of patients. In the absorbed dose differences for rCT- $sCT_{rCT,}$ 7 out of 20 patients were responsible for the outliers in the target and OAR structures

The DVH differences for 13 out of 20 patients, 11 out of 16 patients, and 1 out of 16 patients for rCT-sCT_{rCT}, rCT-$sCT_{CBCT,}$ and rCT-dCBCT were within the acceptable 2.0% dose differences. The rest of

the patients resulted in higher (over 2.0%) dose differences for any dosimetry metric due to incorrect image deformations and erroneously generated sCTs because of anatomical changes.

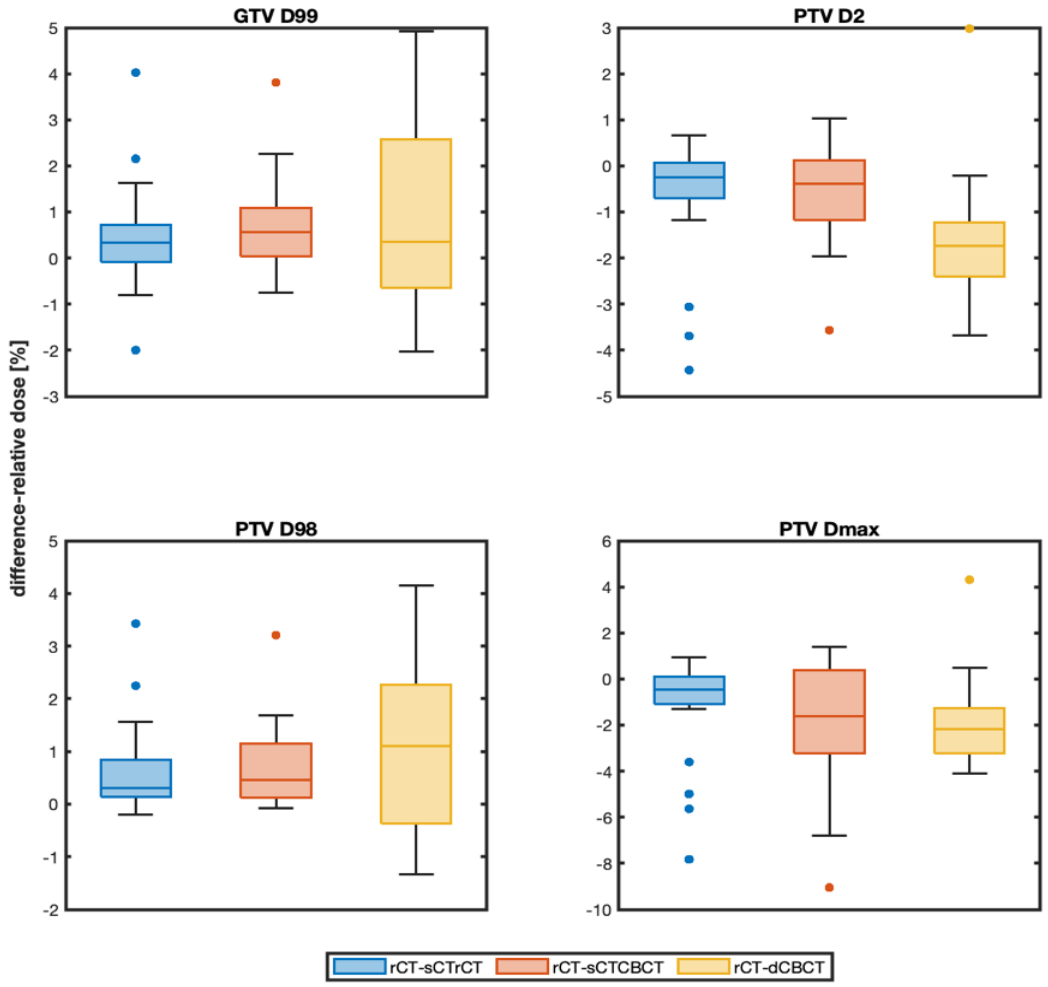

Figure 20: Boxplot with percentual differences of the dose, rCT target DVH metric values subtracted from sCT_{rCT} (blue, n = 20), sCT_{CBCT} (red, n = 16) and dCBCT (yellow, n = 16).

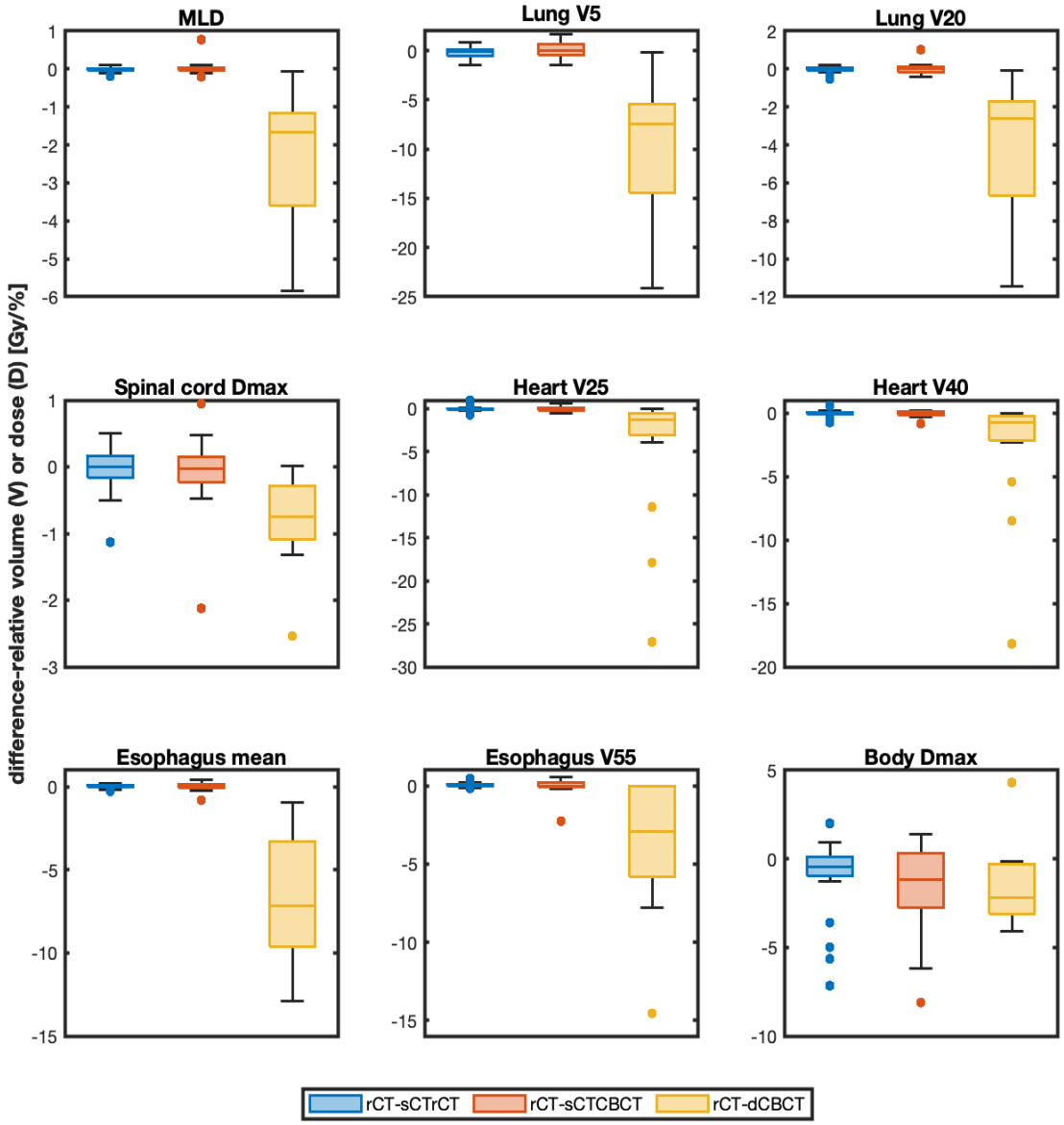

Figure 21: Boxplot with percentual differences of the dose, rCT OAR DVH metric values subtracted from sCT_{rCT} (blue, n = 20), sCT_{CBCT} (red, n = 16) and dCBCT (yellow, n = 16).

4.3 Gamma rate analysis

Gamma rate analysis was conducted to investigate dose distribution between two plans using a pass fraction and gamma map. The gamma rate analysis with criteria 2%/2mm and local gamma rate analysis were executed to compare rCT with sCT_{rCT}, sCT_{CBCT}, and dCBCT, respectively (Table 3).
The gamma evaluation resulted in a mean [min; max] passing rate for the sCT_{rCT} against rCT 98.5% [88.5; 100]%, the sCT_{CBCT} against rCT 94.9% [79.6; 100]%, and the dCBCT against rCT 90.2% [64.0; 99.9]%.

Table 3: Gamma evaluation passing rate when comparing rCT with dCBCT, sCT_{rCT}, and sCT_{CBCT} and the mean gamma passing rate. The gamma criteria were set to 2%/2mm, local gamma rate analysis.

	Pass fraction [%] with 2%/2mm criteria		
PTN	**dCBCT**	**sCT_{rCT}**	**sCT_{CBCT}**
1	98.0	99.1	98.9
2	90.4	100	100
3	64.0	99.1	75.0
4	93.9	99.5	99.6
5	99.4	100	98.0
6	72.8	96.8	79.6
7	94.0	97.2	92.6
8	95.1	99.1	97.9
9	94.1	98.5	96.5
10	80.3	88.5	80.0
11	98.8	100	99.7
12	71.6	99.6	98.4
13	95.1	100	96.1
14	100	99.4	99.0
15	95.5	97.5	97.1
16	93.0	100	97.1
17	94.5	99.9	99.2
18	89.3	95.7	95.7
19	91.68	100	99.6
20	91.79	99.85	99.3
Mean	90.2	98.5	94.9

5. Discussion

There is an interest in implementing oART for lung cancer patients, but uncertainty with sCT generation due to large anatomical changes has caused some clinical concerns. The goal of this study was to investigate if the use of direct dose calculation on CBCT will reduce dosimetric uncertainties compared to the daily use of sCT in an AI-driven CBCT-guided oART for lung cancer patients with large anatomical changes. Unfortunately, large geometrical differences between CBCT and rCT images resulted in a large uncertainty in rCT-dCBCT compared to rCT-sCTs. However, using sCTs for absolute dose calculation is not ideal due to anatomical disagreement between rCT and sCTs images, which caused a dose deviation of over 2.0% in some cases.
The future investigation could include CBCT-like images from the raw rCT data, using simulated CBCT generated from deforming CBCT to rCT or degrading rCT image to mimic CBCT. Implementing CBCT-technique with better HU-definition and bigger FOV is approaching Herlev Hospital clinic. Thus, the use of CBCT as rCT will make the comparison with sCT with the input from the daily CBCT adequate for the same anatomy.

5.1 sCT image evaluation

sCTs generated in Ethos were able to simulate small anatomical changes. However, a particular type of anatomical change during the time interval between pCT and rCT can be too large for the generated sCT to simulate correctly.

The sCT can simulate tumor shrinkage from the outer tissue layer well. In contrast, with a characteristic anatomical change such as "cheese holes" in tumor shrinkage or tumor dispersion, the sCTs had difficulty replicating these changes. This kind of anatomical change was not replicable in the sCT due

to the morphological characters that appeared in the rCT, or the CBCT image was not present in the pCT, highlighting one of the limitations of density mapping in Ethos therapy.
As a result, the generation of the sCT image from Ethos was neither close to the original pCT nor the rCT, but a mixture of both, displayed in patients 6 (Figure 12),7 (Figure 13), and 17 (Figure 14).

Patient 10 (Figure 16), with the appearance of pneumonitis and anatomical change in tumor deviation position on the primary target, the sCT had difficulty simulating the primary tumor on the thoracic wall. It could be due to the combined effect of both anatomical changes affecting the simulation of the area and resulting in a poor target generation in sCT. Similarly, patient 13 with tumor positional deviation caused an incorrect simulation of the tumor position in the sCT (Figure 17).

The time duration between pCT and CBCT post-re-planning (in days to weeks) or rCT and CBCT post-re-planning (in a few days) illustrates the unpredictable nature of anatomical change for lung cancer patients. The CBCT was not acquired on the same day as rCT led risk of anatomical disagreement between rCT and CBCT, which affected the simulation of sCT. Four out of 20 patients in this project had an anatomical disagreement between rCT and CBCT, despite having just 2-5 days between the image accusation. The sCT_{CBCT} was generated from deforming pCT to CBCT. There is a possibility that if oART is clinically implemented for lung cancer patients and the appearance of atelectasis, pleural effusion, or pneumonitis occurs during the course of treatment, a re-scan CT is necessary for a correctly sCT simulation of the new anatomy. However, the appearance of conditions could resolve on their own during treatment and likely cause another anatomical change.

In addition, the generation of sCT in Ethos therapy occurs in the background and is presented for the user when the plan report is generated in step 4 in the oART workflow (Figure 2) with a 2D view of a sCT slice. As a result, it is difficult to evaluate the generated sCT image quality during the treatment. The only way to visualize sCT in 3D volume is in Mobius 3D, the independent dose verification software used for QA. In summary, the limitation of density mapping and sCT generation should be considered as the main issue that needs to be solved before moving forward with oART for lung patients with Ethos therapy.

5.2 Dose comparison analysis

The Wilcoxon statical test revealed a statistically significant difference between rCT and sCT_{rCT} for the PTV and body structure. At the same time, the rCT and sCT_{CBCT} had a statistically significant difference for GTV, PTV, and body structures. The anatomical disagreements between the sCTs and rCT images were the cause. The comparison of the median absorbed dose for the target structures and body structures (Table 2) was within the acceptable dose difference of 2.0%. The 3D gamma evaluation (using 2%/2mm local gamma criteria) gave a mean passing rate of 98.5%, 94.9% and, 90.2%, respectively, for the dose distributions calculated on sCT_{rCT}, sCT_{CBCT} and, dCBCT compared to rCT. It was found that dose calculation on sCTs at an occurrence of anatomical change was better than expected; however, the presence of several outliers indicates that it is not feasible to rely on the accuracy of dose calculation on sCTs generated from deforming the pCT to the image of the anatomy-of-the-day. The result of this project has demonstrated it is more difficult to conclude whether oART for lung cancer patients is more dose-sparing for OAR due to the large anatomical disagreement. It also depends on each case of the anatomical change, where one type of anatomical change is not representative of other patients with the same type of anatomical change.

Ideally, the CBCT and rCT images should be acquired within the same day to eliminate the anatomical change between the two occasions and different geometrical information from the two image modalities. However, since this is a retrospective study, image acquisition within the same day was impossible, and rigid image registration was used to compensate for the geometrical differences between the two image modalities. The rigid image registration was likely also the cause of the outliers (Figure 20, Figure 21) and an insufficient image registration method for this project.

In general, the DVH parameters or median value for rCT- sCT_{CBCT} was slightly worse than rCT- sCT_{rCT} and had a larger variability, especially for the target and body structure, which was expected. However,

the DVH of OAR structure for rCT-sCT_{rCT} and rCT-sCT_{CBCT} were almost identical, with less than 1% dose disagreement.

The result from dose comparison for anatomical disagreement between the sCT and rCT did not always cause a dose difference larger than 2.0%. Therefore, the dose differences for all DVH parameters must be carefully observed for each lung cancer patient.

13 out of 20 patients and 11 out of 16 patients for rCT-sCT_{rCT} and rCT- sCT_{CBCT} were within the 2.0% dose difference. Patients 6, 7, 10, 14, 15, 18, and 19 caused outliers in rCT-sCT_{rCT}, where 6 of 7 patients had noticeable anatomical differences between rCT and sCT_{rCT}. Patient 6 caused the highest target dose difference with -7.8% and -9.0% for PTV D_{max} for rCT-sCT_{rCT} and rCT- sCT_{CBCT}, respectively. Patient 10 in rCT-sCT_{rCT} caused a -5.6% absorbed dose difference in PTV D_{max}. A tendency of a higher absorbed dose for PTV D_{max} in the sCTs re-calculation plan was observed, even for patient 19, with a good anatomical agreement between rCT and sCT (*Appendix B: Patient images*).
The dose difference can be as large as -7.8% and -9.0% for target structure in rCT-sCT_{rCT} and rCT-sCT_{CBCT}. It proves the necessity of a patient and fraction-specific QA to implement lung cancer patients in oART clinically, and it is not feasible to rely on sCT dose calculation accuracy.

Brahme et al. [48] stated that dose distribution in a few hundred patients with less than $\pm$10% for uncertainty in tumor control probability and less than $\pm$7% is preferable but recommended 3% to commonly access dose uncertainties. The re-calculated sCT_{rCT} and sCT_{CBCT} were within Brahme et al. recommendation dose uncertainty. The difficulties with this study were to draw a general conclusion due to different tumor locations, treatment approaches, and delivered doses. The 2.0% acceptance level was deliberately chosen despite different endpoints for organs and targets to have a generalized standard. Therefore, the dose comparison analysis in the study should be taken with a grain of salt due to the harsh acceptance level. Nevertheless, this study set an acceptance level at 2%, which was deemed more reasonable since the study only observed dose differences between two image sets without introducing dosimetric and measurement uncertainties.

The approach to implementing oART for lung cancer without the uncertainty with sCT is the direct dose calculation on the daily CBCT. The poor image quality and different geometry caused unexpectedly large dose disagreement between rCT and dCBCT. Studies by Cole et al.[38] demonstrate the potential use of direct dose calculation on CBCT with an appropriate approach, such as simulated CBCT, to minimize the geometry between rCT and CBCT. As mentioned in *section 2.3*, Cole et al. demonstrated a maximum dose difference of less than 2.0% for the target and OAR within this study's acceptable range.

In this study, one can entertain the idea of the potential dose sparing for one outlier patient, which could benefit from the direct dose calculation approach. Patient 6 dose difference was -1.1% for PTV D_{max} in rCT-dCBCT, which is 6.7% less than the absorbed dose calculation on the rCT-sCT_{rCT} with -7.8%. Hence, the direct calculation on CBCT also resulted in a higher dose difference for OAR, such as for the lung, heart, and esophagus. No general conclusions can be drawn for the direct dose calculation on CBCT since the geometry of the CBCT and rCT were different. As a result, the direct calculation on a CBCT needs further investigation.

6. Conclusion

In conclusion, large anatomical changes could cause dose deviations larger than 2.0% due to incorrect image deformation and generation of sCT; however, it was not always the case. Despite the anatomical difference between rCT and sCT, the dose differences were within 2%. It indicated a need for a patient and fraction-specific QA for clinical implementation of lung cancer in oART, which is unavailable for the current treatment system.
The use of direct dose calculation on CBCT for lung cancer patients needs further investigation. The geometric differences between rCT and CBCT were too large, and this study could not conclude.

7. Future perspective

Conducting direct dose calculation on CBCT is a potentially feasible solution and needs further investigation. However, one needs an appropriate approach to commercial solutions to implement direct dose calculation on CBCT. The newest release of Varian Hypersight is a promising tool to combat this problem.

Another approach to investigate the use of direct calculation on CBCT images could be the usage of a "fake" CBCT. This could be done by degrading the image quality of the rCT image to mimic a CBCT image or a simulated CBCT to minimize the geometric differences.

Another interesting aspect of this project would be the re-optimization of the plan with the deformed structure propagated in sCT. This study mainly focused on re-calculating plans without re-optimizing due to time limitations.

8. Reference

[1] Schabath MB, Cote ML. Cancer Progress and Priorities: Lung Cancer. *Cancer Epidemiol Biomarkers Prev* 2019; 28: 1563–1579.

[2] de Groot P, Munden RF. Lung cancer epidemiology, risk factors, and prevention. *Radiol Clin North Am* 2012; 50: 863–876.

[3] Lemjabbar-Alaoui H, Hassan OUI, Yang YW, et al. Lung cancer: Biology and treatment options. *Biochim Biophys Acta* 2015; 1856: 189–210.

[4] Vinod SK, Hau E. Radiotherapy treatment for lung cancer: Current status and future directions. *Respirology* 2020; 25: 61–71.

[5] Belderbos J, van Beek S, van Kranen S, et al. Anatomical Changes During Radiotherapy of Lung Cancer Patients. *International Journal of Radiation Oncology*Biology*Physics* 2007; 69: S508–S509.

[6] Chargari C, Riet F, Mazevet M, et al. Complications of thoracic radiotherapy. *Presse Med*; 42. Epub ahead of print 2013. DOI: 10.1016/J.LPM.2013.06.012.

[7] Banfill K, Giuliani M, Aznar M, et al. Cardiac Toxicity of Thoracic Radiotherapy: Existing Evidence and Future Directions. *J Thorac Oncol* 2021; 16: 216–227.

[8] Chang JY, Gomez DR. Adaptive Radiation for Lung Cancer. *J Oncol*; 2011. Epub ahead of print 2011. DOI: 10.1155/2011/898391.

[9] Åström LM, Behrens CP, Calmels L, et al. Online adaptive radiotherapy of urinary bladder cancer with full re-optimization to the anatomy of the day: Initial experience and dosimetric benefits. *Radiotherapy and Oncology* 2022; 171: 37–42.

[10] Zwart LGM, Ong F, ten Asbroek LA, et al. Cone-beam computed tomography-guided online adaptive radiotherapy is feasible for prostate cancer patients. *Phys Imaging Radiat Oncol* 2022; 22: 98.

[11] Sibolt P, Andersson LM, Calmels L, et al. Clinical implementation of artificial intelligence-driven cone-beam computed tomography-guided online adaptive radiotherapy in the pelvic region. *Phys Imaging Radiat Oncol* 2021; 17: 1–7.

[12] Åström LM, Behrens CP, Storm KS, et al. Online adaptive radiotherapy of anal cancer: Normal tissue sparing, target propagation methods, and first clinical experience. *Radiotherapy and Oncology* 2022; 176: 92–98.

[13] Shelley CE, Bolt MA, Hollingdale R, et al. Implementing cone-beam computed tomography-guided online adaptive radiotherapy in cervical cancer. *Clin Transl Radiat Oncol*; 40. Epub ahead of print 1 May 2023. DOI: 10.1016/J.CTRO.2023.100596.

[14] Hoegen P, Lang C, Akbaba S, et al. Cone-Beam-CT Guided Adaptive Radiotherapy for Locally Advanced Non-small Cell Lung Cancer Enables Quality Assurance and Superior Sparing of Healthy Lung. *Front Oncol* 2020; 10: 2724.

[15] Dial C, Weiss E, Siebers J V., et al. Benefits of adaptive. *Med Phys* 2016; 43: 1787–1794.

[16] Møller DS, Khalil AA, Knap MM, et al. Adaptive radiotherapy of lung cancer patients with pleural effusion or atelectasis. *Radiotherapy and Oncology* 2014; 110: 517–522.

[17] Varian. Ethos^{TM} Therapy: Intelligent Adaptation Comes to the Clinic | Varian, https://www.varian.com/ethostm-therapy-intelligent-adaptation-comes-clinic (accessed 15 May 2023).
[18] Hoffmann L, Persson GF, Nygård L, et al. Thorough design and pre-trial quality assurance (QA) decrease dosimetric impact of delineation and dose planning variability in the STRICTLUNG and STARLUNG trials for stereotactic body radiotherapy (SBRT) of central and ultra-central lung tumours. *Radiotherapy and Oncology* 2022; 171: 53–61.
[19] Palmér E, Karlsson A, Nordström F, et al. Synthetic computed tomography data allows for accurate absorbed dose calculations in a magnetic resonance imaging only workflow for head and neck radiotherapy. *Phys Imaging Radiat Oncol* 2021; 17: 36–42.
[20] Shafai-Erfani G, Wang T, Lei Y, et al. Dose Evaluation of MRI-based Synthetic CT Generated Using a Machine Learning Method for Prostate Cancer Radiotherapy. *Med Dosim* 2019; 44: e64.
[21] Jonsson JH, Karlsson MG, Karlsson M, et al. Treatment planning using MRI data: an analysis of the dose calculation accuracy for different treatment regions. *Radiat Oncol*; 5. Epub ahead of print 30 June 2010. DOI: 10.1186/1748-717X-5-62.
[22] Åström LM, Behrens CP, Storm KS, et al. Online adaptive radiotherapy of anal cancer: Normal tissue sparing, target propagation methods, and first clinical experience. *Radiotherapy and Oncology* 2022; 176: 92–98.
[23] Oh S, Kim S. Deformable image registration in radiation therapy. *Radiat Oncol J* 2017; 35: 101–111.
[24] Shackleford J, Kandasamy N, Sharp G. High-performance deformable image registration algorithms for manycore processors. *High-Performance Deformable Image Registration Algorithms for Manycore Processors* 2013; 1–114.
[25] Patrikalakis NM, Maekawa T, Cho W. 1.4.2 B-spline curve. *Massachusetts Institute of Technology*, https://web.mit.edu/hyperbook/Patrikalakis-Maekawa-Cho/node17.html (2009, accessed 3 May 2023).
[26] Wu Z, Lan T, Wang J, et al. Medical Image Registration Using B-Spline Transform. DOI: 10.5013/IJSSST.a.17.48.01.
[27] Rohr K. Elastic Registration of Multimodal Medical Images: A Survey. *KI* 2000; 14: 11–17.
[28] Broit C. Optimal registration of deformed images.
[29] Omer OA, Tanaka T. Robust image registration based on local standard deviation and image intensity. *2007 6th International Conference on Information, Communications and Signal Processing, ICICS*. Epub ahead of print 2007. DOI: 10.1109/ICICS.2007.4449748.
[30] Bajcsy R. Multiresolution Elastic Matching*. *Comput Vis Graph Image Process* 1989; 46: 1–21.
[31] Kumar M, Shanavas M, Sidappa A, et al. Cone Beam Computed Tomography - Know its Secrets. *J Int Oral Health* 2015; 7: 64.
[32] Villard PF, Fournier G, Beuve M, et al. Visualisation of physical lung simulation: An interactive application to assist physicians. *Proceedings - International Conference on Medical Information Visualisation - BioMedical Visualisation, MediVis 2006* 2006; 65–70.
[33] Albarakati H, Jackson P, Gulal O, et al. Dose assessment for daily cone-beam CT in lung radiotherapy patients and its combination with treatment planning. *Phys Eng Sci Med* 2022; 45: 231–237.
[34] Gong H, Liu B, Zhang G, et al. Evaluation of Dose Calculation Based on Cone-Beam CT Using Different Measuring Correction Methods for Head and Neck Cancer Patients. *Technol Cancer Res Treat*; 22. Epub ahead of print 1 January 2023. DOI: 10.1177/15330338221148317/ASSET/IMAGES/LARGE/10.1177_15330338221148317-FIG5.JPEG.
[35] De Smet M, Schuring D, Nijsten S, et al. Accuracy of dose calculations on kV cone beam CT images of lung cancer patients. *Med Phys* 2016; 43: 5934–5941.
[36] Kaplan LP, Elstrøm UV, Møller DS, et al. Cone beam CT based dose calculation in the thorax region. *Phys Imaging Radiat Oncol* 2018; 7: 45–50.

[37] Fotina I, Hopfgartner J, Stock M, et al. Feasibility of CBCT-based dose calculation: Comparative analysis of HU adjustment techniques. *Radiotherapy and Oncology* 2012; 104: 249–256.
[38] Cole AJ, Veiga C, Johnson U, et al. Toward adaptive radiotherapy for lung patients: feasibility study on deforming planning CT to CBCT to assess the impact of anatomical changes on dosimetry. *Phys Med Biol*; 63. Epub ahead of print 31 July 2018. DOI: 10.1088/1361-6560/AAD1BB.
[39] Atelectasis: Causes, Symptoms, Diagnosis & Treatment, https://my.clevelandclinic.org/health/diseases/17699-atelectasis (accessed 15 February 2023).
[40] Pneumonia - Symptoms and causes - Mayo Clinic, https://www.mayoclinic.org/diseases-conditions/pneumonia/symptoms-causes/syc-20354204 (accessed 15 February 2023).
[41] Merrick C, Asciak R, Edey A, et al. Pleural Effusion. *ERS Monograph* 2023; 2018: 64–74.
[42] Low DA, Harms WB, Mutic S, et al. A technique for the quantitative evaluation of dose distributions. *Med Phys* 1998; 25: 656–661.
[43] Park JM, Kim JI, Park SY, et al. Reliability of the gamma index analysis as a verification method of volumetric modulated arc therapy plans. *Radiation Oncology* 2018; 13: 1–14.
[44] ClinicalTrials.gov. Novel Approach to Radiotherapy in Locally Advanced Lung Cancer Concomitant Navelbine®, https://clinicaltrials.gov/ct2/show/NCT02354274?term=NARLAL2&cond=Lung+Cancer&cntry=DK&draw=2&rank=1 (accessed 21 May 2023).
[45] Møller DS, Nielsen TB, Brink C, et al. Heterogeneous FDG-guided dose-escalation for locally advanced NSCLC (the NARLAL2 trial): Design and early dosimetric results of a randomized, multi-centre phase-III study. *Radiotherapy and Oncology* 2017; 124: 311–317.
[46] Hoffmann L, Knap MM, Khalil AA, et al. The NARLAL2 dose escalation trial: dosimetric implications of inter-fractional changes in organs at risk. *https://doi.org/101080/0284186X20171366049* 2017; 57: 473–479.
[47] Khan Academy. Box plot review (article) | Khan Academy, https://www.khanacademy.org/math/statistics-probability/summarizing-quantitative-data/box-whisker-plots/a/box-plot-review (accessed 8 November 2023).
[48] Brahme A. Dosimetric precision requirements in radiation therapy. *Acta Radiol Oncol* 1984; 23: 379–391.

Appendix A : Patient information

Table 4:Patient information with description of re-scanning causes, diagnosis, fraction number of CBCT post-re-scanning, and time duration between re-scan CT and CBCTar acquisition.

Patient	Re-planning causes	Treatment type	CBCTar fraction	Time duration [d]
1	Resolution of atelectasis	NSCLC66	FX 11	5
2	Tumor shrinkage	NSCLC66	FX 14	4
3	Resolution of atelectasis	NSCLC66	FX 6	3
4	Resolution of atelectasis	NSCLC66	FX 4	1
5	Tumor positional deviation	NSCLC66	FX 17	3
6	Tumor shrinkage	NSCLC66	FX 24	1
7	Tumor dispersion	NSCLC66	FX 18	2
8	Tumor shrinkage	NSCLC95	FX 5	2
9	Tumor shrinkage	NSCLC66	FX 14	2
10	Tumor positional deviation and pneumonitis	SCLC50	FX 19	2
11	Tumor positional deviation	SCLC45	FX 6	3
12	Resolution of atelectasis	SCLC45	FX 7	1
13	Tumor positional deviation (GTV-T) and Tumor positional shift (GTV-N), pleural effusion, and pneumonitis	SCLC45	FX 18	4
14	Tumor enlargement	SBRT67.5	FX 2	3
15	Resolution of atelectasis	NSCLC66	FX 17	3
16	Tumor shrinkage	NSCLC66	FX 21	1
17	Tumor shrinkage	SCLC45	FX 22	4
18	Tumor shrinkage	NSCLC66	FX 19	4
19	Tumor positional deviation and shrinkage	NSCLC95	FX 12	3
20	Tumor shrinkage	NSCLC66	FX 19	4

Appendix B : Patient images

Patient 8 (TS): Moderate anatomical disagreement inside GTV, where the sCT is closer to pCT than rCT, caused the outlier.

pCT

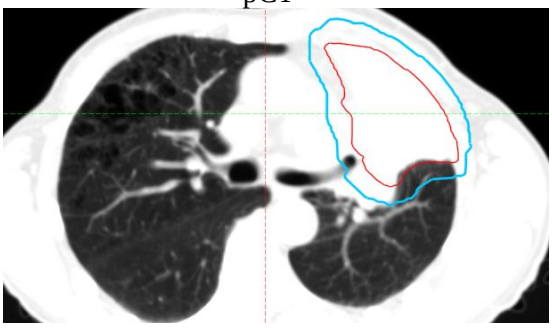

rCT(green) vs. sCT_{rCT} (magenta)

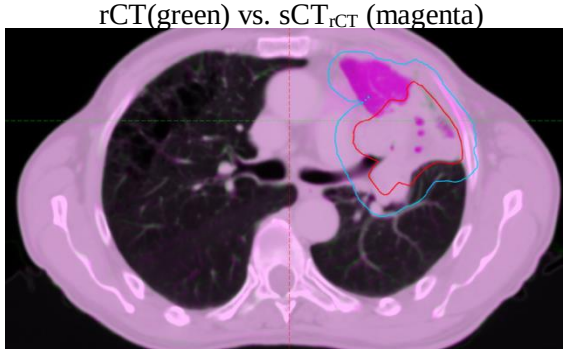

CBCT

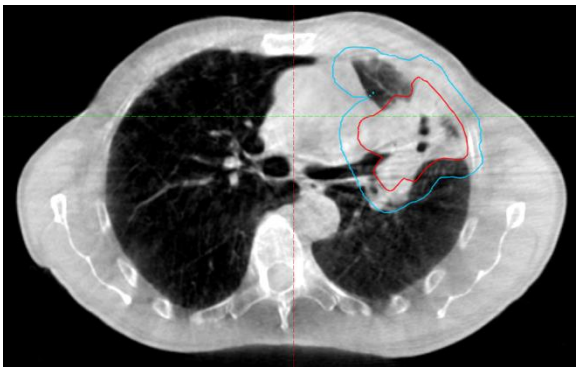

rCT(green) vs. sCT_{CBCT} (magenta)

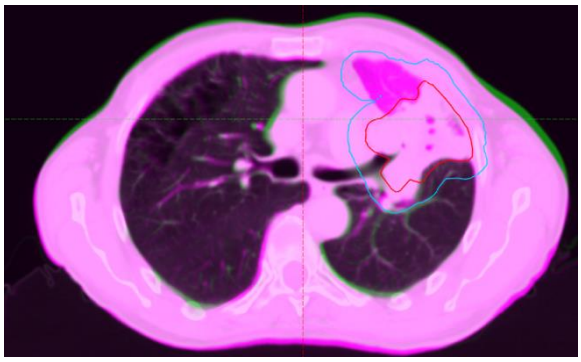

Patient 9 (TS): Moderate anatomical disagreement; the sCT did not handle the tumor shrinkage on the thorax wall well and caused the outlier.

pCT

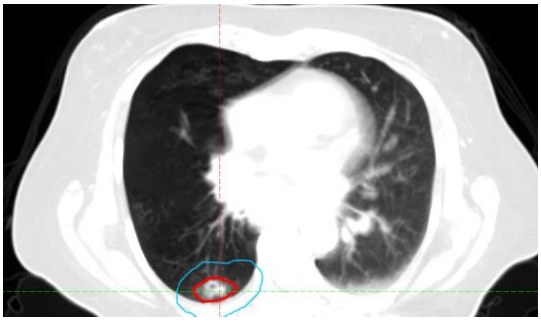

rCT(green) vs. sCT_{rCT} (magenta)

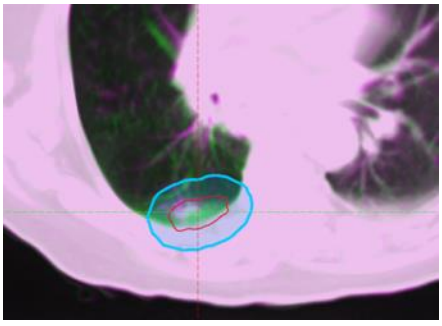

CBCT

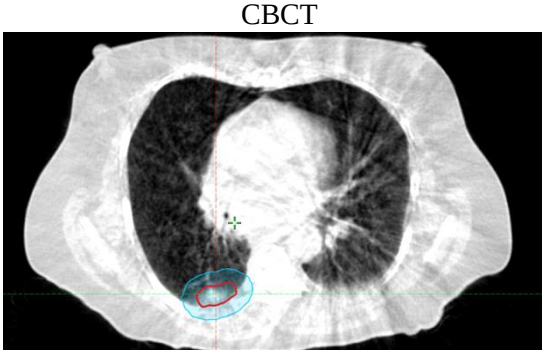

rCT(green) vs. sCT_{CBCT} (magenta)

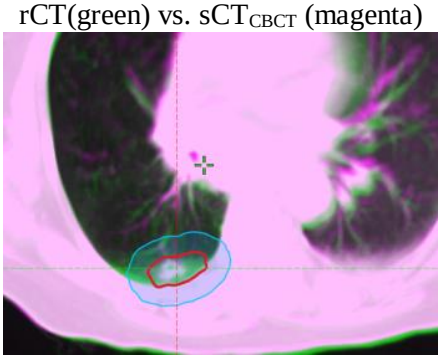

Patient 12 (Ate): Moderate anatomical difference with spinal cord deformation viewed in breast window level, caused no outliers. The sCTs had difficulty replicating the tissue close to the spinal cord.

pCT

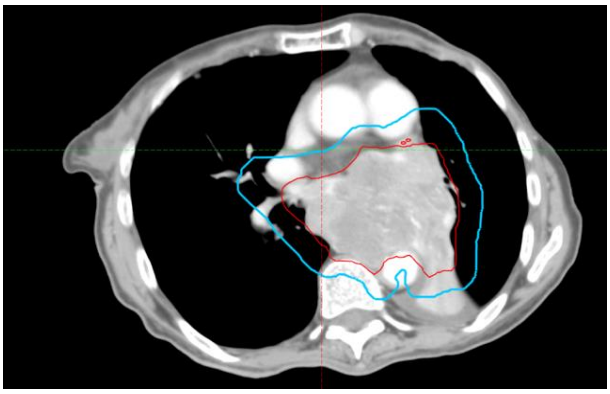

rCT(green) vs. sCT_{rCT} (magenta)

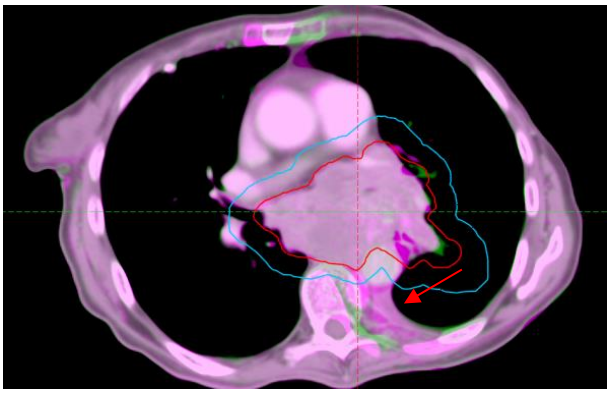

CBCT

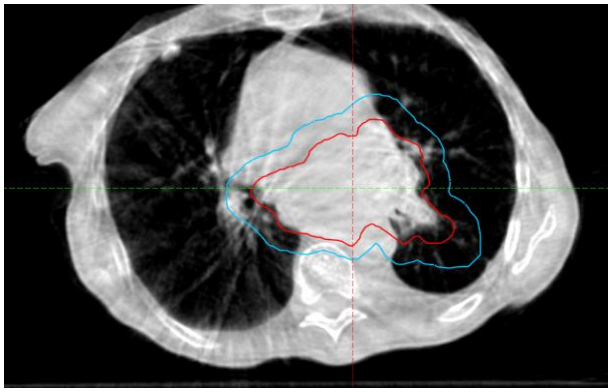

rCT(green) vs. sCT_{CBCT} (magenta)

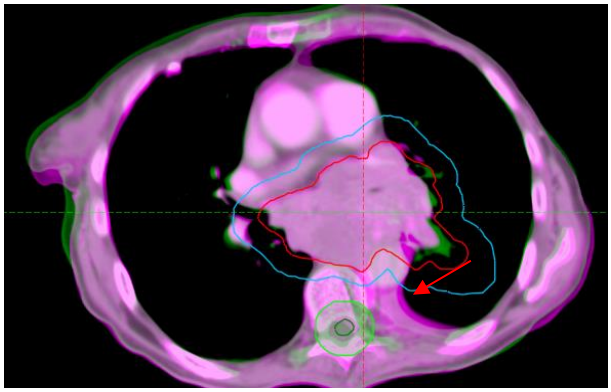

Patient 14 (Tumor enlargement): Small anatomical disagreement, where the tumor on rCT was slightly larger than sCTs, caused an outlier.

pCT

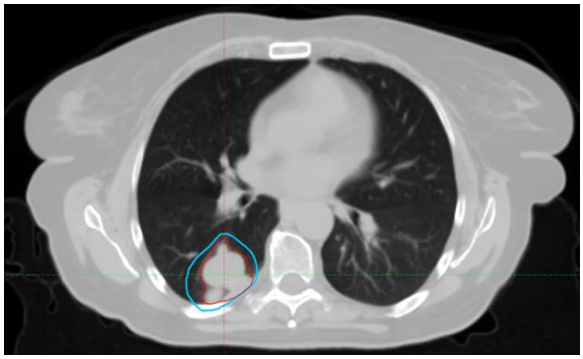

rCT(green) vs. sCT_{rCT} (magenta)

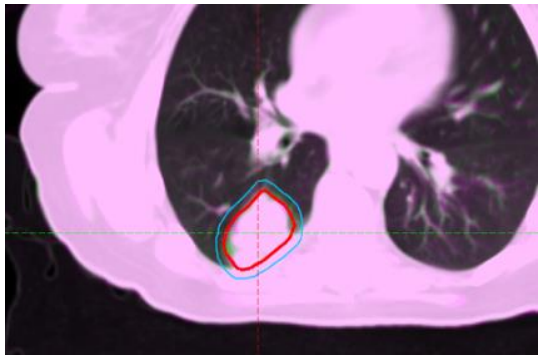

CBCT

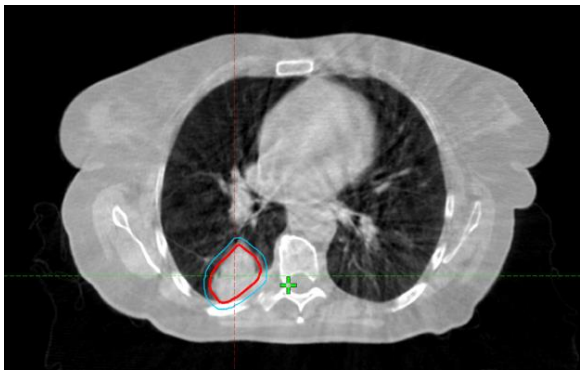

rCT(green) vs. sCT_{CBCT} (magenta)

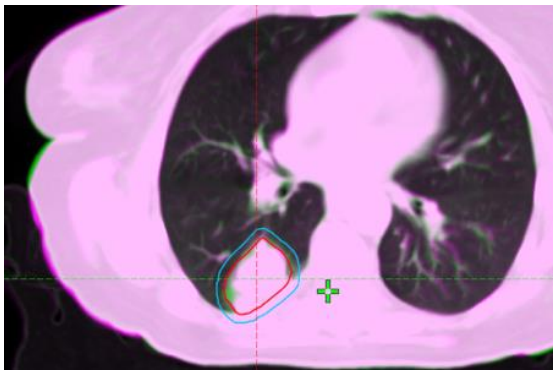

Patient 15 (Ate): Moderate anatomical disagreement, where the tumor inside GTV was smaller in rCT than sCT, caused an outlier.

pCT

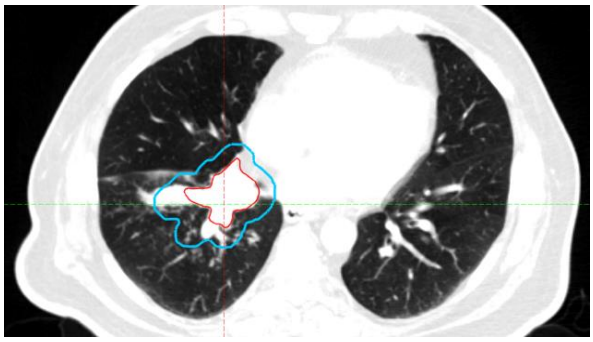

rCT(green) vs. sCT_{rCT} (magenta)

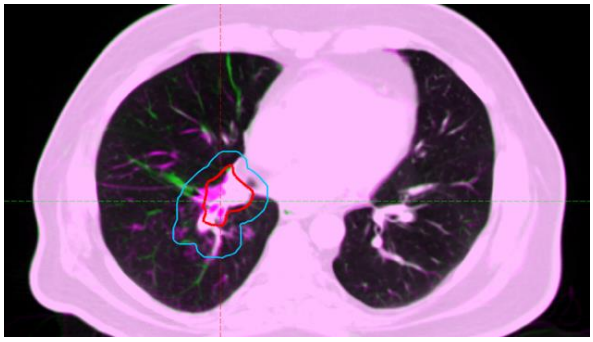

CBCT

rCT(green) vs. sCT_{CBCT} (magenta)

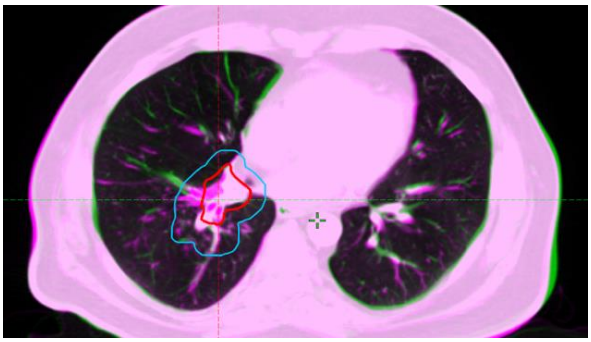

Patient 16 (TS): Small anatomical differences inside the GTV structure caused no outliers.

pCT

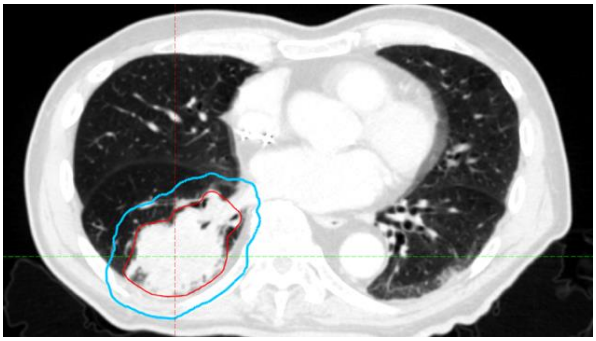

rCT(green) vs. sCT_{rCT} (magenta)

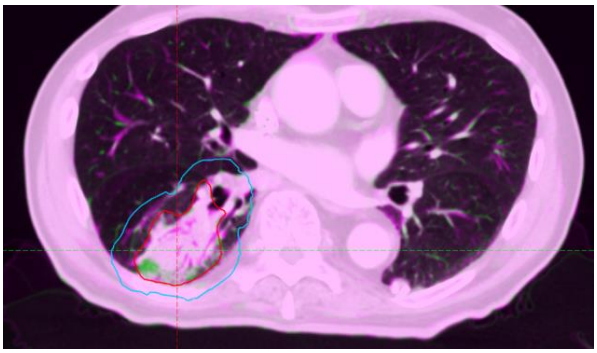

CBCT

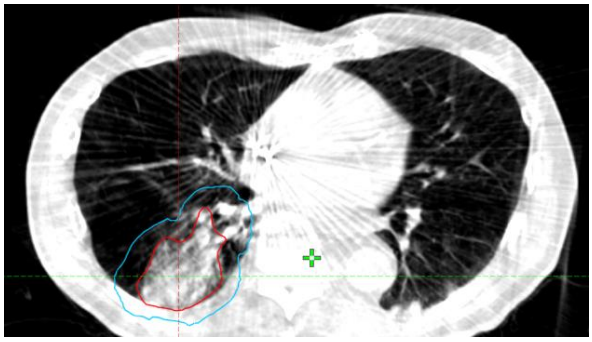

rCT(green) vs. sCT_{CBCT} (magenta)

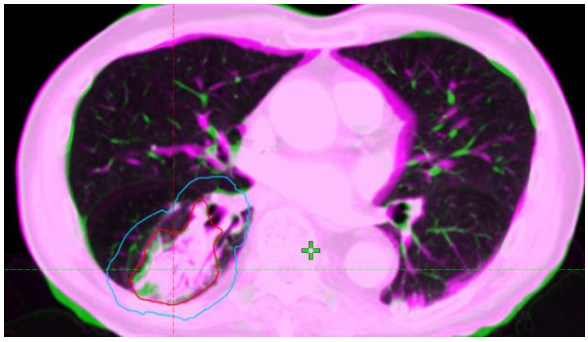

Patient 18 (TS): Small anatomical disagreement inside the GTV structure caused an outlier.

pCT

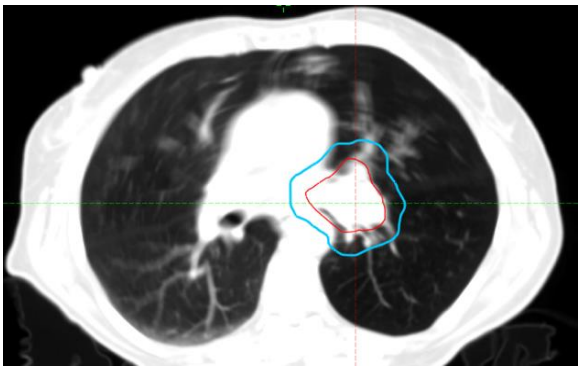

rCT(green) vs. sCT_{rCT} (magenta)

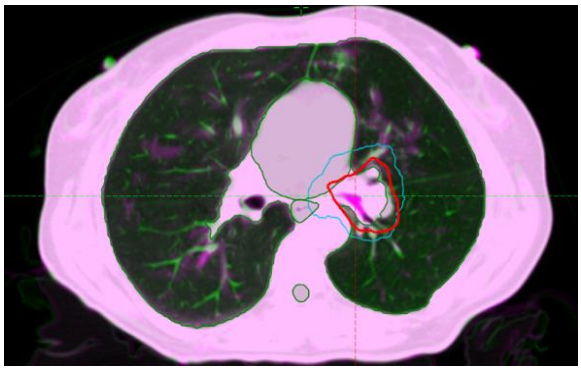

CBCT

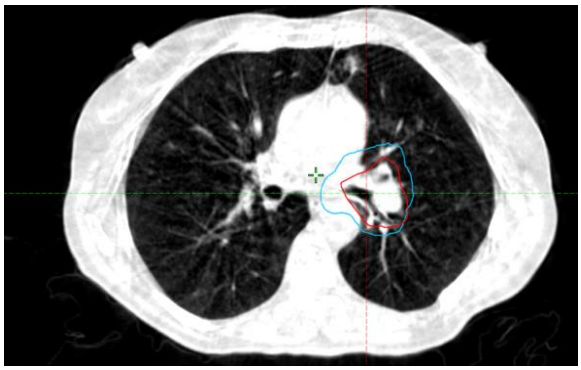

rCT(green) vs. sCT_{CBCT} (magenta)

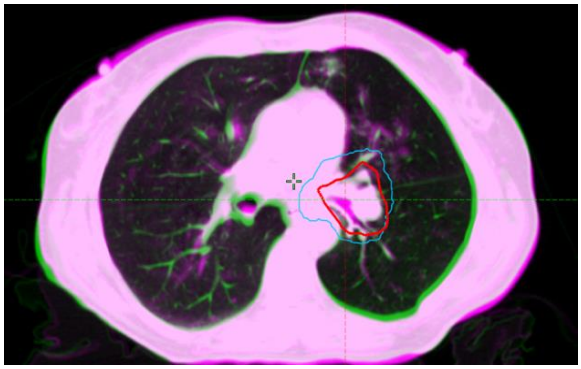

Patient 19 (TPD and TS): Anatomical agreement between rCT and sCT_{rCT} caused outlier dose difference for rCT-sCT_{rCT} with -5.0% for PTV D_{max}.

pCT

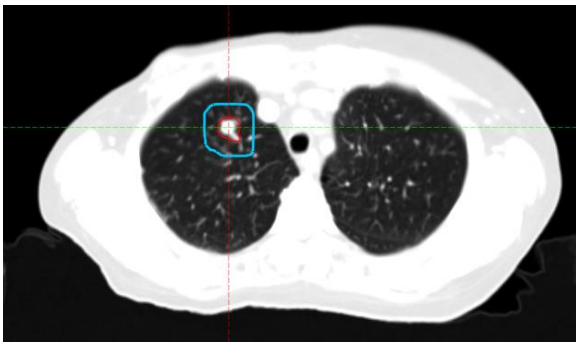

rCT(green) vs. sCT_{rCT} (magenta)

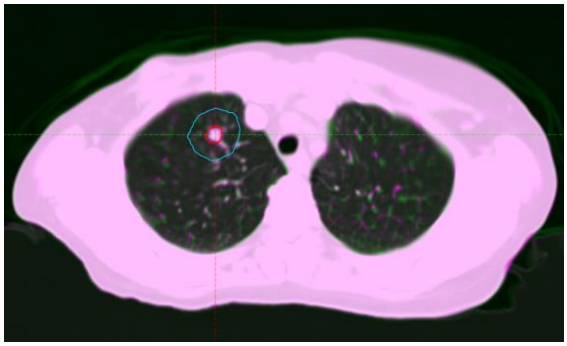

CBCT

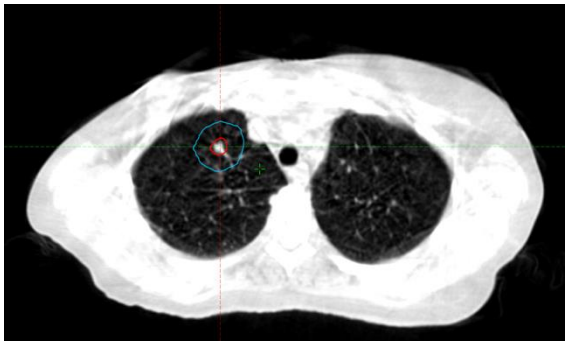

rCT(green) vs. sCT_{CBCT} (magenta)